

---

---

**Excited state spectroscopy in the lattice  
Gross-Neveu Model**

---

---

**Julia Danzer**

Diplomarbeit  
zur Erlangung des Grades  
Magistra der Naturwissenschaften

Institut für Physik, Fachbereich Theoretische Physik  
Karl-Franzens Universität Graz

unter Anleitung von  
Prof. Dr. Christof Gattringer

Institut für Physik, Fachbereich Theoretische Physik  
Karl-Franzens Universität Graz

Graz, September 2007



# Abstract

We investigate the lattice Gross-Neveu model in  $1 + 1$  dimensions in a dynamical simulation for various numbers of flavors. Our motivation is excited state spectroscopy on the lattice, and the improvement of it. As the main tool we use the variational method, which provides the excited states out of a correlation matrix built from a set of interpolators with the quantum numbers of the states one is interested in.

The central idea is to introduce new types of interpolators, which we construct from field variables distributed on different lattice points. Furthermore, relative minus signs allow for derivative-type sources.

We find that some of the excited states are scattering states which we distinguish from bound states by their volume dependence.

Our analysis extends also to simulations with different numbers of flavors which is easy to implement in the Hybrid Monte-Carlo algorithm used here. This is interesting since at large  $N_f$  analytic results for the Gross-Neveu model are available.

The experience with excited lattice spectroscopy obtained in this study might be useful when analysing resonances in full QCD simulations. A first account of our results was published in [1].



# Contents

<b>1</b>	<b>Introduction</b>	<b>1</b>
<b>2</b>	<b>The Gross-Neveu model</b>	<b>5</b>
2.1	The action of the Gross-Neveu model . . . . .	5
2.2	Symmetries of the model . . . . .	7
2.3	The Gross-Neveu model in the large $N_f$ limit . . . . .	9
<b>3</b>	<b>Lattice formulation</b>	<b>11</b>
3.1	Euclidean correlators in the continuum . . . . .	11
3.2	The path integral for Euclidean correlators . . . . .	12
3.3	The path integral for scalar fields . . . . .	14
3.4	Lattice regularisation . . . . .	15
<b>4</b>	<b>Wilson fermions</b>	<b>19</b>
4.1	The lattice Gross-Neveu action . . . . .	19
4.2	Key formulas for fermions on the lattice . . . . .	22
4.3	The free case $g = 0$ . . . . .	24
4.4	Spectrum of the Dirac operator . . . . .	25
<b>5</b>	<b>Numerical simulations</b>	<b>29</b>
5.1	Monte-Carlo simulations on the lattice . . . . .	29
5.1.1	Central idea of Monte-Carlo simulations . . . . .	29
5.1.2	Markov chain . . . . .	30
5.1.3	The reweighting algorithm for the Gross-Neveu model . . . . .	31
5.2	Techniques for dynamical Fermions . . . . .	32
5.3	Hybrid Monte-Carlo algorithm . . . . .	33
5.3.1	The molecular dynamics leapfrog evolution . . . . .	33

5.3.2	Implementing HMC for the Gross-Neveu model . . . . .	34
<b>6</b>	<b>Interpolators and their symmetries</b>	<b>37</b>
6.1	Wick's theorem . . . . .	38
6.2	Derivative sources . . . . .	39
6.3	Symmetries and quantum numbers . . . . .	41
6.3.1	Parity . . . . .	41
6.3.2	Time reflection . . . . .	43
6.3.3	Charge conjugation . . . . .	43
<b>7</b>	<b>Excited state spectroscopy</b>	<b>47</b>
7.1	The variational method . . . . .	47
7.2	Effective masses . . . . .	49
7.3	Fit of the correlator . . . . .	51
<b>8</b>	<b>Evaluation of the data - results</b>	<b>53</b>
8.1	Diagonal correlators . . . . .	54
8.2	Effective mass plateaus . . . . .	54
8.3	Choice of interpolators . . . . .	59
8.4	Mass dependence of the spectrum . . . . .	60
8.5	Finite size effects - scattering states . . . . .	61
8.6	The eigenvectors of the eigenvalue problem . . . . .	64
8.7	Extrapolation of the mass spectrum . . . . .	67
8.8	Interpretation of the results . . . . .	69
8.9	Table for the mass values . . . . .	74
<b>9</b>	<b>Summary and outlook</b>	<b>75</b>
<b>A</b>	<b>Fourier transformation on the lattice</b>	<b>79</b>
<b>B</b>	<b>The 2-dimensional representation of the <math>\gamma</math>-matrices</b>	<b>81</b>
<b>C</b>	<b>Discussion of the correlation matrix</b>	<b>83</b>
	<b>References</b>	<b>85</b>

# Chapter 1

## Introduction

Nowadays Quantum chromodynamics (QCD) on the lattice is a well established field. In recent years there have been huge conceptual breakthroughs and also the computer technology has improved considerably. This pushed the research immensely forward and good quantitative results start to come in.

However, it is still a major problem in lattice QCD to extract excited particle masses out of 2-point functions. While the numerical ground state spectroscopy is well under control, the excited states are not. On the other hand, lots of experimental data on excitations of hadrons exist from particle accelerators. Unfortunately, reproducing the spectrum of hadronic excitations is a highly non-trivial task. As a matter of fact, obtaining the complete hadron spectrum out of numerical calculations, would be a strong test for the correctness of QCD. Hence a comparison of the experimental and numerical data for excitations, would be of high interest.

As mentioned, excited state spectroscopy is hard for the lattice. The reason for that is, that the excitations appear as subleading terms in the Euclidean correlators. Hence, it is not easy to extract them. However, a powerful method exists. The idea is to build a correlation matrix with as many interpolators as possible, where all interpolator have the quantum numbers of the state, one is interested in. The order of the matrix roughly corresponds to the number of states one can get out. But, as said before, the excited states are just subleading terms in the matrix. However, considerable improvement has been obtained with the introduction of the variational method [2, 3]. It allows for a clean extraction of the excited states from the correlation matrix.

Furthermore, there exist finite volume techniques for distinguishing bound- and scattering states.

As remarked, the techniques are known, but the problem is that they are hard to implement in full QCD. Large volumes are necessary, which are very expensive numerically. Furthermore, the principles for the construction of the interpolators are often unclear.

Moreover, the role of dynamical fermions for excitations has not been studied. The dynamical fermions include the fermion determinant in the calculations, whereas until now mainly quenched simulations, which means setting the fermion determinant equal to one, have been done. Including the fermion determinant brings in all contributions from sea quarks. In particular, now creation of quark-antiquark pairs is possible, which allows for the decay of excited states. The quenched simulations ignore exactly those vacuum fluctuations and no decay is possible. This is why dynamical simulations for excited states would be of high interest.

The goal of this diploma thesis is to test the known lattice techniques for excited states in a simple  $1 + 1$ -dimensional lattice field theory, the Gross-Neveu (GN) model. It is an asymptotically free, renormalisable model with a four-fermi interaction. To use lower dimensional models is quite a common way of approaching problems in theoretical physics. Important lessons for the more complicated and more expensive QCD simulations can be learned. The hope is to gain insights, which can be later applied in  $3 + 1$  dimensions.

In this work the studied topics are the construction of the interpolators with the correct quantum numbers of the state one is interested in. With them we can build large correlation matrices. Then we analyse the effects of dynamical quarks, since up to now, there have mainly been only quenched simulations. We are also interested in the methods for distinguishing scattering states from bound states, using finite volume studies. Furthermore we investigate the properties of the Gross-Neveu model in general, such as the flavor dependence of the results. We hope to make contact to large  $N_f$  results [4, 5].

This thesis is organised as follows: The continuum form of the GN model and its symmetries are discussed in Chap. 2. Important is that the four-fermi interaction is broken up over a Hubbard-Stratonovich [6, 7] transformation, which introduces a scalar field. The path integral on the lattice is established in Chap. 3.

Also the formulas for Euclidean 2-point functions are presented there. Chap. 4 deals with the lattice formulation of the GN model, Wilson fermions and some key formulas for the Grassmann valued fermion fields.

The generation of the scalar fields will be done with a dynamical simulation, which includes the fermion determinant. The numerical implementation is achieved with the Hybrid Monte-Carlo algorithm (HMC). The adaption of this algorithm to the GN model is a large part of this thesis. In the end, the HMC will allow us to work with arbitrary even numbers of flavors, which is one of the points of interest in this work. The necessary numerical and theoretical steps will be presented in Chap. 5.

As we already know, the correlation technique is only good if we use a large set of interpolators. Our central idea is to construct them by distributing the interpolators over several lattice points. This means we do not put all sources at the same place, but rather shift them relative to each other. The methods of the construction of the interpolators and the quantum numbers are discussed in Chap. 6.

The tool to extract the excited states is the variational method. It uses the generalised eigenvalue problem. The underlying ideas are presented in Chap. 7, which also contains a description of our analysis techniques.

The plots of the results will be presented and discussed in Chap. 8. In the final evaluation of the data we also investigate finite size effects. The analysis of the volume dependence will show, that also scattering states play an important role in the spectrum. In Chap. 8 the emerging physical picture will be addressed.

Finally, in Chap. 9 a summary is given which collects the most important results, and speculates, what further steps for improvement of the analysis could be done.



# Chapter 2

## The Gross-Neveu model

The model we consider contains  $N_f$  flavors of fermions with a local quartic fermi interaction in two space-time dimensions. It is one of the simplest, renormalisable, asymptotically free models [8]. We will present now the explicit form as well as some symmetries of this model.

### 2.1 The action of the Gross-Neveu model

The action of the two-dimensional model is given by

$$S[\bar{\psi}, \psi, \Phi] = \int d^2x \mathcal{L}[\bar{\psi}, \psi, \Phi] , \quad (2.1)$$

with the Lagrangian density  $\mathcal{L}$ ,

$$\mathcal{L}[\bar{\psi}, \psi, \Phi] = \sum_{f=1}^{N_f} \bar{\psi}^{(f)}(\mathbf{x}) [\gamma_\mu \partial_\mu + m^{(f)} + \sqrt{g} \Phi(\mathbf{x})] \psi^{(f)}(\mathbf{x}) + \frac{1}{2} \Phi^2(\mathbf{x}) . \quad (2.2)$$

The index  $f$  runs over all flavors.  $\psi$  and  $\bar{\psi}$  are two-component fermion fields,

$$\psi^{(f)}(\mathbf{x}) = ( \psi_1^{(f)}(\mathbf{x}) , \psi_2^{(f)}(\mathbf{x}) )^T , \quad (2.3)$$

$$\bar{\psi}^{(f)}(\mathbf{x}) = ( \bar{\psi}_1^{(f)}(\mathbf{x}) , \bar{\psi}_2^{(f)}(\mathbf{x}) ) . \quad (2.4)$$

The field  $\Phi$  is a real scalar field,  $g$  is the coupling constant and the mass matrix  $m^{(f)}$  is defined as

$$m^{(f)} = \text{diag} \left( m^{(1)}, m^{(2)}, \dots , m^{(N_f)} \right) . \quad (2.5)$$

A possible representation of the two-dimensional Euclidean Dirac  $\gamma$ -matrices is

$$\begin{aligned}\gamma_0 &= \begin{pmatrix} 1 & 0 \\ 0 & 1 \end{pmatrix}, & \gamma_1 &= \begin{pmatrix} 0 & 1 \\ 1 & 0 \end{pmatrix}, \\ \gamma_2 &= \begin{pmatrix} 0 & -i \\ i & 0 \end{pmatrix}, & \gamma_5 &= \begin{pmatrix} 1 & 0 \\ 0 & -1 \end{pmatrix}.\end{aligned}\quad (2.6)$$

These are nothing but the Pauli matrices  $\sigma_0, \sigma_1, \sigma_2, \sigma_3$ . The chirality operator is  $\gamma_5$  and the parity operator is  $\gamma_2$ , since we define 2 to be the Euclidean time direction. The partition function of the system is a path integral over the fermion fields  $\bar{\psi}$  and  $\psi$  as well as over the scalar field  $\Phi$  and is given by

$$Z_{GN} = \int D[\bar{\psi}, \psi, \Phi] e^{-S[\bar{\psi}, \psi, \Phi]}.\quad (2.7)$$

The integration measure  $D[\bar{\psi}, \psi, \Phi]$  over all field configurations has only a formal meaning in the continuum, but will be made precise when we switch to the lattice formulation.

We now perform a *Hubbard-Stratonovich* [6, 7] transformation which reformulates the interacting fermion system on the lattice by integrating out the auxiliary field  $\Phi$ . We obtain

$$Z_{GN} = \int D[\bar{\psi}, \psi, \Phi] e^{-S[\bar{\psi}, \psi, \Phi]} \longrightarrow Z_{GN} = \int D[\bar{\psi}, \psi] e^{-S_{\text{eff}}[\bar{\psi}, \psi]}.\quad (2.8)$$

The key identity of this transformation is the Gaussian integral

$$(2\pi)^{-\frac{1}{2}} \int dx \exp\left(-\frac{1}{2}x^2 - xA\right) = \exp\left(-\frac{1}{2}A^2\right).\quad (2.9)$$

This transformation leads to the effective action

$$\begin{aligned}S_{\text{eff}}[\bar{\psi}, \psi] &= \int d^2x \left( \sum_{f=1}^{N_f} \bar{\psi}^{(f)}(\mathbf{x}) [\gamma_\mu \partial_\mu + m^{(f)}] \psi^{(f)}(\mathbf{x}) \right. \\ &\quad \left. - \frac{g}{2} \left[ \sum_{f=1}^{N_f} \bar{\psi}^{(f)}(\mathbf{x}) \psi^{(f)}(\mathbf{x}) \right]^2 \right),\end{aligned}\quad (2.10)$$

where the 4-fermi character of the interaction is manifest.

## 2.2 Symmetries of the model

The Gross-Neveu (GN) model has some important symmetries [9]. First of all each term in the action (2.10) is invariant under the continuous global  $U(1)$  symmetry

$$\psi(\mathbf{x}) \longrightarrow \exp(i\alpha) \psi(\mathbf{x}) , \quad \bar{\psi}(\mathbf{x}) \longrightarrow \bar{\psi}(\mathbf{x}) \exp(-i\alpha) . \quad (2.11)$$

If the fermion mass  $m$  vanishes, it is also invariant under the discrete global chiral  $Z_2$  transformation

$$\psi^{(f)}(\mathbf{x}) \longrightarrow \gamma_5 \psi^{(f)}(\mathbf{x}) , \quad \bar{\psi}^{(f)}(\mathbf{x}) \longrightarrow -\bar{\psi}^{(f)}(\mathbf{x}) \gamma_5 . \quad (2.12)$$

The relation (2.11) is obvious. The second transformation (2.12) uses the anti-commuting properties of the  $\gamma$  matrices

$$\gamma_i \gamma_j + \gamma_j \gamma_i = 0 . \quad (2.13)$$

The kinetic part gives

$$\begin{aligned} \bar{\psi}^{(f)}(\mathbf{x}) \gamma_\mu \partial_\mu \psi^{(f)}(\mathbf{x}) &\longrightarrow -\bar{\psi}^{(f)}(\mathbf{x}) \gamma_5 \gamma_\mu \partial_\mu \gamma_5 \psi^{(f)}(\mathbf{x}) \\ &= -\bar{\psi}^{(f)}(\mathbf{x}) \gamma_5 \gamma_\mu \gamma_5 \partial_\mu \psi^{(f)}(\mathbf{x}) \\ &= \bar{\psi}^{(f)}(\mathbf{x}) \gamma_5 \gamma_5 \gamma_\mu \partial_\mu \psi^{(f)}(\mathbf{x}) \\ &= \bar{\psi}^{(f)}(\mathbf{x}) \gamma_\mu \partial_\mu \psi^{(f)}(\mathbf{x}) . \end{aligned} \quad (2.14)$$

For the quartic fermion interaction the symmetry transformation works the same way. The term  $\bar{\psi}^{(f)}(\mathbf{x}) \psi^{(f)}(\mathbf{x})$  however, changes its sign under this transformation. Consequently the action of Eq. (2.10) is only invariant if the mass vanishes.

The global chiral  $Z_2$  symmetry is a special case of the continuous chiral transformation

$$\psi^{(f)}(\mathbf{x}) \longrightarrow e^{i\theta\gamma_5} \psi^{(f)}(\mathbf{x}) , \quad \bar{\psi}^{(f)}(\mathbf{x}) \longrightarrow -\bar{\psi}^{(f)}(\mathbf{x}) e^{i\theta\gamma_5} . \quad (2.15)$$

$\theta$  is a real parameter, and for  $\theta = \pi/2$  we find Eq.( 2.12). Again the mass term breaks this symmetry, and the kinetic term remains invariant. For the symmetry of the interaction we have to distinguish two cases. The one flavor case  $N_f = 1$  and the situation with  $N_f > 1$ .

First we consider the one-flavor case. We apply the transformation to the interaction term which then reads

$$\begin{aligned}
[\bar{\psi}(\mathbf{x}) \psi(\mathbf{x})]^2 &\longrightarrow [\bar{\psi}(\mathbf{x}) e^{2i\theta\gamma_5} \psi(\mathbf{x})]^2 \\
&= [\bar{\psi}(\mathbf{x}) (\cos(2\theta) + i\gamma_5 \sin(2\theta)) \psi(\mathbf{x})]^2 \\
&= [\bar{\psi}(\mathbf{x}) \psi(\mathbf{x})]^2 \cos^2(2\theta) - [\bar{\psi}(\mathbf{x}) \gamma_5 \psi(\mathbf{x})]^2 \sin^2(2\theta) \\
&\quad + 2i \cos(2\theta) \sin(2\theta) \bar{\psi}(\mathbf{x}) \psi(\mathbf{x}) \bar{\psi}(\mathbf{x}) \gamma_5 \psi(\mathbf{x}) \\
&= [\bar{\psi}(\mathbf{x}) \psi(\mathbf{x})]^2 .
\end{aligned} \tag{2.16}$$

We used the nilpotency of the fermion fields  $\psi_i^2 = \bar{\psi}_i^2 = 0$  and the identity

$$\begin{aligned}
[\bar{\psi}(\mathbf{x}) \psi(\mathbf{x})]^2 &= [\bar{\psi}_1(\mathbf{x}) \psi_1(\mathbf{x}) + \bar{\psi}_2(\mathbf{x}) \psi_2(\mathbf{x})]^2 \\
&= 2 \bar{\psi}_1(\mathbf{x}) \psi_1(\mathbf{x}) \bar{\psi}_2(\mathbf{x}) \psi_2(\mathbf{x}) \\
&= -[\bar{\psi}_1(\mathbf{x}) \psi_1(\mathbf{x}) - \bar{\psi}_2(\mathbf{x}) \psi_2(\mathbf{x})]^2 \\
&= -[(\bar{\psi}_1(\mathbf{x}), \bar{\psi}_2(\mathbf{x})) \gamma_5 (\psi_1(\mathbf{x}), \psi_2(\mathbf{x}))^T]^2 \\
&= -[\bar{\psi}(\mathbf{x}) \gamma_5 \psi(\mathbf{x})]^2 .
\end{aligned} \tag{2.17}$$

There exists also a third form, known from the *Thirring model* [10], which is for  $N_f = 1$  equal to our interaction.

$$\begin{aligned}
&-\frac{1}{2} \left[ \sum_{\mu=1}^2 \bar{\psi}(\mathbf{x}) \gamma_\mu \psi(\mathbf{x}) \right]^2 \\
&= -\frac{1}{2} [(\bar{\psi}_1(\mathbf{x}) \psi_2(\mathbf{x}) + \bar{\psi}_2(\mathbf{x}) \psi_1(\mathbf{x}))^2 + (-i\bar{\psi}_1(\mathbf{x}) \psi_2(\mathbf{x}) + i\bar{\psi}_2(\mathbf{x}) \psi_1(\mathbf{x}))^2] \\
&= -\bar{\psi}_1(\mathbf{x}) \psi_2(\mathbf{x}) \bar{\psi}_2(\mathbf{x}) \psi_1(\mathbf{x}) - \bar{\psi}_1(\mathbf{x}) \psi_2(\mathbf{x}) \bar{\psi}_2(\mathbf{x}) \psi_1(\mathbf{x}) \\
&= 2 \bar{\psi}_1(\mathbf{x}) \psi_1(\mathbf{x}) \bar{\psi}_2(\mathbf{x}) \psi_2(\mathbf{x}) \\
&= [\bar{\psi}(\mathbf{x}) \psi(\mathbf{x})]^2 .
\end{aligned} \tag{2.18}$$

To summarise for  $N_f = 1$ , we have three equivalent forms of the interaction term which are

$$[\bar{\psi}(\mathbf{x}) \psi(\mathbf{x})]^2 = -[\bar{\psi}(\mathbf{x}) \gamma_5 \psi(\mathbf{x})]^2 = -\frac{1}{2} [\bar{\psi}(\mathbf{x}) \gamma_\mu \psi(\mathbf{x})]^2 , \tag{2.19}$$

and all three of them are invariant under the continuous transformation (2.15).

Next we look at the  $N_f > 1$  case. Here the identity (2.17) cannot be used and in order to construct an invariant interaction term we add two four-Fermi terms,

which leads to a *Nambu-Lasinio-type model* [11, 12]. The interaction here reads

$$\left( \sum_{f=1}^{N_f} \bar{\psi}^{(f)}(\mathbf{x}) \psi^{(f)}(\mathbf{x}) \right)^2 - \left( \sum_{f=1}^{N_f} \bar{\psi}^{(f)}(\mathbf{x}) \gamma_5 \psi^{(f)}(\mathbf{x}) \right)^2 . \quad (2.20)$$

Performing the continuous chiral transformation shows that now the interaction is invariant under (2.15).

In this diploma thesis calculations for the correlation function will be performed for even values of  $N_f$ . A continuous symmetry as in Eq. (2.15) can not be broken spontaneously in 2 dimensions, a fact known as the *Mermin-Wagner theorem* [13]. The absence of spontaneous symmetry breaking in two-dimensional systems was rigorously proven by Coleman in quantum field theory [14] and by Mermin, Wagner and Hohenberg in statistical physics [15]. On the other hand discrete symmetries can be broken in 2 dimensions. Since we are interested in the spontaneous breaking we restrict ourselves to the interaction as given in (2.10).

## 2.3 The Gross-Neveu model in the large $N_f$ limit

We are interested in calculating the particle mass spectrum in the Gross-Neveu model. Some analytical calculations can be done in the large  $N_f$  limit [4, 5], since for large  $N_f$  the model is asymptotically free. Gross and Neveu found that  $\bar{\psi}\psi$  develops a vacuum expectation value where the symmetry (2.12) is broken spontaneously. In the process, the dimensionless coupling constant  $g$  is traded for an arbitrary dimensional parameter  $g \langle \bar{\psi}\psi \rangle$ . So the theory contains no dimensionless parameter other than the number of fermions  $N_f$ . Consequently, any physical dimensionless quantity, such as the ratio of two particle masses, can depend only on  $N_f$ . As stated in [4, 5], the result of the excited mass calculation leads to

$$m_n = m_1 \frac{2N_f}{\pi} \sin \left( \frac{n\pi}{2N_f} \right) , \quad (2.21)$$

where  $n$  is the quantum number for the  $n^{\text{th}}$  excited state. Expanding this formula in a power series in  $1/N_f$  we find in leading order

$$m_n = m_1 n , \quad n = 1, 2, \dots < N_f . \quad (2.22)$$

So the excited mass is always an integer multiple of the ground state mass  $m_1$ . Later we will compare our results to this formula.

At this point we remark that a simulation of the  $N_f = 1$  model has been done in the diploma thesis of M. Limmer [16, 17]. His work was particularly helpful in the basic understanding of the GN model and provided us with some background literature.

Further literature about the Gross-Neveu model is given in [18, 19, 20, 21].

# Chapter 3

## Lattice formulation

In the last section we introduced the model we are working with in the continuum formulation. The numerical simulations will be done on a 1 + 1-dimensional lattice. For that we prepare in this chapter by deriving the lattice formulation of a general Euclidean action. In our presentation we follow [22]. Further literature can be found in [23, 24, 25].

### 3.1 Euclidean correlators in the continuum

One of the most important formulas in lattice field theory and the key equation in this diploma thesis are the Euclidean correlation functions. These are defined as

$$\frac{1}{Z_T} \text{Tr} [e^{-(T-t)\hat{H}} \hat{O}_2 e^{-t\hat{H}} \hat{O}_1] . \quad (3.1)$$

$Z_T = \text{Tr} [\exp(-T\hat{H})]$  is a normalisation factor, the so-called *partition function*.  $\hat{H}$  is the Hamiltonian,  $\hat{O}_1, \hat{O}_2$  are the two operators we want to correlate and  $t, T$  are real numbers with  $T > t$  (Euclidean time). By inserting eigenstates of  $\hat{H}$ , the correlator can be written as

$$\lim_{T \rightarrow \infty} \frac{1}{Z_T} \text{Tr} [e^{-(T-t)\hat{H}} \hat{O}_2 e^{-t\hat{H}} \hat{O}_1] = \sum_n \langle 0 | \hat{O}_2 | n \rangle \langle n | \hat{O}_1 | 0 \rangle e^{-tE_n} . \quad (3.2)$$

The sum in Eq. (3.2) runs over all physical states  $|n\rangle$ . Each operator  $\hat{O}_i$  is sandwiched between the vacuum state  $|0\rangle$  and a physical state  $|n\rangle$ . These matrix elements are multiplied with a time-dependent weight factor containing the energy

eigenvalues  $E_n$  in the exponent. From the exponential decay as a function of time  $t$ , the energies  $E_n$  can be extracted. In our second formulation of this equation we write the correlation function as a path integral

$$\frac{1}{Z_T} \text{Tr}[e^{-(T-t)\hat{H}} \hat{O}_2 e^{-t\hat{H}} \hat{O}_1] = \frac{1}{Z_T} \int D[\Phi] e^{-S_E[\Phi]} O_2[\Phi(.,t)] O_1[\Phi(.,0)] . \quad (3.3)$$

Here the integral is over all possible configurations of the field  $\Phi$ . The operators on the right-hand side are now functionals and the exponent is the Boltzmann weight which contains the Euclidean action. The functionals in Eq. (3.3) are evaluated for the fields  $\Phi(.,0)$ , with time argument 0, and  $\Phi(.,t)$  with the time argument  $t$ . The dot for the spatial argument expresses, that the functionals map the whole field configuration, defined by the set of all field values at the given time, into the complex numbers.

We are going to evaluate the r.h.s. of Eq. (3.3) on the lattice by using Monte Carlo techniques. But first, a derivation of the path integral formulation will be presented.

## 3.2 The path integral for Euclidean correlators

The energy of a quantum mechanical system is described by the Hamiltonian

$$\hat{H} = \frac{\hat{p}^2}{2m} + \hat{U} , \quad (3.4)$$

which consists of the kinetic and the potential energy. When quantising the system, the position  $x$  and the momentum  $p$ , become operators. They do not commute with each other but obey the following relation,

$$[\hat{x}, \hat{p}] = i . \quad (3.5)$$

In this notation we set  $\hbar = 1$  and it will be also suppressed in the continuing formulas. The momentum operator  $\hat{p}$  can be written as the derivative with respect to the position

$$\hat{p} = -i \frac{\partial}{\partial x} . \quad (3.6)$$

The partition function is

$$\text{Tr}[e^{-T\hat{H}}] = \int dx \langle x | e^{-T\hat{H}} | x \rangle . \quad (3.7)$$

We first consider the case where the potential is equal to zero, so that we deal with a free particle. We compute the matrix element

$$\langle x|e^{-t\hat{H}}|y\rangle = \int dp \langle x|e^{-t\frac{p^2}{2m}}|p\rangle\langle p|y\rangle. \quad (3.8)$$

Using  $\hat{p}|p\rangle = p|p\rangle$  and  $\langle x|p\rangle = \frac{1}{\sqrt{2\pi}}e^{ipx}$  we find

$$\int dp \langle x|p\rangle\langle p|y\rangle e^{-t\frac{p^2}{2m}} = \frac{1}{2\pi} \int dp e^{ip(x-y)} e^{-t\frac{p^2}{2m}} = \sqrt{\frac{m}{2\pi t}} e^{-(x-y)^2\frac{m}{2t}}. \quad (3.9)$$

In the last step we just solved the Gaussian integral. Now we reintroduce the potential energy. In order to be able to calculate that second part we decompose the time into infinitesimal steps  $\epsilon$ , such that

$$e^{-\epsilon\hat{H}} = e^{-\frac{\epsilon}{2}\hat{U}} e^{-\frac{\epsilon}{2}\hat{H}_0} e^{-\frac{\epsilon}{2}\hat{U}} [1 + \mathcal{O}(\epsilon)] = \hat{W}_\epsilon [1 + \mathcal{O}(\epsilon)]. \quad (3.10)$$

We again regard the matrix element of Eq. (3.8), which now changes to

$$\langle x|\hat{W}_\epsilon|y\rangle = e^{-\frac{\epsilon}{2}U(x)} \langle x|e^{-\epsilon\hat{H}_0}|y\rangle e^{-\frac{\epsilon}{2}U(x)} = \sqrt{\frac{m}{2\pi\epsilon}} e^{-\frac{\epsilon}{2}U(x)} e^{-(x-y)^2\frac{m}{2\epsilon}} e^{-\frac{\epsilon}{2}U(x)}. \quad (3.11)$$

In the last part of our derivation of the partition function we apply the *Trotter formula*

$$e^{-T\hat{H}} = \lim_{N_T \rightarrow \infty} (\hat{W}_\epsilon)^{N_T}, \quad N_T \epsilon = T. \quad (3.12)$$

So the partition function becomes

$$\begin{aligned} Z_T &= \text{Tr} e^{-T\hat{H}} = \int dx_0 \langle x_0|e^{-T\hat{H}}|x_0\rangle = \lim_{N_T \rightarrow \infty} \int dx_0 \langle x_0|(\hat{W}_\epsilon)^{N_T}|x_0\rangle \\ &= \lim_{N_T \rightarrow \infty} \int dx_0 dx_1 \dots dx_{N_T-1} \langle x_0|\hat{W}_\epsilon|x_1\rangle \langle x_1|\hat{W}_\epsilon|x_2\rangle \dots \langle x_{N_T-1}|\hat{W}_\epsilon|x_0\rangle \\ &= \lim_{N_T \rightarrow \infty} c^{N_T} \int_{-\infty}^{\infty} dx_0 \dots dx_{N_T-1} e^{-\frac{\epsilon}{2}U(x_0)} e^{-(x_0-x_1)^2\frac{m}{2\epsilon}} e^{-\frac{\epsilon}{2}U(x_1)} e^{\frac{\epsilon}{2}U(x_0)} \dots \\ &\quad \dots e^{-\frac{\epsilon}{2}U(x_{N_T-1})} e^{-(x_{N_T-1}-x_0)^2\frac{m}{2\epsilon}} e^{-\frac{\epsilon}{2}U(x_0)} \\ &= \lim_{N_T \rightarrow \infty} c^{N_T} \int_{-\infty}^{\infty} dx_0 \dots dx_{N_T-1} \exp\left(-\epsilon \sum_{j=1}^{N_T-1} \left(\frac{m}{2} \frac{(x_j - x_{j+1})^2}{\epsilon^2} \right. \right. \\ &\quad \left. \left. + U(x_j)\right)\right), \end{aligned} \quad (3.13)$$

with the abbreviation  $c = \sqrt{m/(2\pi\epsilon)}$  and the identification  $x_{N_T} = x_0$ . Since the number of steps  $N_T$  has to be finite in a numerical evaluation we define an approximation of the partition function

$$Z_T^\epsilon = c^{N_T} \int_{-\infty}^{\infty} dx_0 \dots dx_{N_T-1} \exp \left( -\epsilon \sum_{j=1}^{N_T-1} \left( \frac{m}{2} \frac{(x_j - x_{j+1})^2}{\epsilon^2} + U(x_j) \right) \right). \quad (3.14)$$

In this equation we identify in the exponent the so-called Euclidean action  $S_E$ , which is obtained from the usual action  $S$  when we introduce the imaginary time  $t = i\tau$ , so that we end up with

$$\begin{aligned} S[x, \dot{x}] &= \int_0^T d\tau \left( \frac{m}{2} \dot{x}(\tau)^2 - U(x(\tau)) \right) \\ &\longrightarrow i \int_0^T dt \left( \frac{m}{2} \dot{x}(t)^2 - U(x(t)) \right) = iS_E[x, \dot{x}]. \end{aligned} \quad (3.15)$$

We have constructed an approximation for the partition function  $Z_T^\epsilon$  which is given as an integral over a Boltzmann factor with the Euclidean action  $S_E$ . The integral is called a path integral, because the collection of values  $x_j$  can be interpreted as a discretised path, and the integral is over all possible paths. In the next section we will derive the path integral formalism for a scalar field, but first summarise the expression for a 2-point function as

$$\langle \hat{x}(t)\hat{x}(0) \rangle = \frac{\int \prod_{i=1}^{N_T-1} dx_i e^{-S_E[x_i]} x_{n_i} x_0}{\int \prod_{i=1}^{N_T-1} dx_i e^{-S_E[x_i]}}. \quad (3.16)$$

### 3.3 The path integral for scalar fields

The action in Minkowski space is defined as

$$S = \int dt dx \mathcal{L} [\Phi(t, x), \partial_\mu \Phi(t, x)], \quad (3.17)$$

where  $\mathcal{L}$  is the Lagrangian density with

$$\mathcal{L} [\Phi, \partial_\mu \Phi] = \frac{1}{2} (\partial_\mu \Phi)(\partial^\mu \Phi) - \frac{m^2}{2} \Phi^2 - V(\Phi). \quad (3.18)$$

The first part is the kinetic term and  $V(\Phi)$  is a potential. By using the Euler-Lagrange equations

$$\partial_\mu \left( \frac{\partial \mathcal{L}}{\partial (\partial_\mu \Phi)} \right) - \frac{\partial \mathcal{L}}{\partial \Phi} = 0, \quad (3.19)$$

we obtain

$$(\square + m^2)\Phi = -V'(\Phi) . \quad (3.20)$$

This is the equation of motion, which is the Klein-Gordon equation with a potential. Now we quantise our system by using the canonical formalism. We introduce the canonical momentum

$$\pi(x, t) = \frac{\partial}{\partial \dot{\Phi}(x, t)} \mathcal{L}(\Phi, \partial_\mu \Phi) = \dot{\Phi}(x, t) , \quad (3.21)$$

and the Hamiltonian

$$H = \int dx \pi(x, t) \dot{\Phi}(x, t) - \int d^2x \mathcal{L}(\Phi(x, t), \partial_\mu \Phi(x, t)) . \quad (3.22)$$

The classical fields are replaced by operators obeying the commutation relations

$$[\hat{\Phi}(x), \hat{\pi}(y)] = i \delta(x - y), \quad [\hat{\Phi}(x), \hat{\Phi}(y)] = [\hat{\pi}(x), \hat{\pi}(y)] = 0 . \quad (3.23)$$

### 3.4 Lattice regularisation

We introduce a regulator by discretising our system on the lattice. Since here we aim at a 1 + 1-dimensional Euclidean theory, we depart from a 1-dimensional space which we discretise so that

$$x \longrightarrow a \cdot n_1 . \quad (3.24)$$

$n_1$  numbers the lattice sites and runs over  $n_1 = 0, \dots, N - 1$ .  $a$  is the lattice spacing. The equal time commutator relations change to

$$[\hat{\Phi}(n_1), \hat{\pi}(m_1)] = i a^{-1} \delta_{n_1, m_1}, \quad [\hat{\Phi}(n_1), \hat{\Phi}(m_1)] = [\hat{\pi}(n_1), \hat{\pi}(m_1)] = 0 . \quad (3.25)$$

The derivative is replaced by a finite difference

$$\partial_x \hat{\Phi}(x) \longrightarrow \frac{\hat{\Phi}(n_1 + 1) - \hat{\Phi}(n_1 - 1)}{2a} , \quad (3.26)$$

with an error of order  $\mathcal{O}(a^2)$ . Furthermore

$$\hat{\pi}(n_1) = -\frac{i}{a} \frac{\partial}{\partial \Phi(n_1)} , \quad (3.27)$$

such that the Hamiltonian becomes

$$\hat{H} = a \sum_{n_1 \in \Lambda_1} \left[ \frac{1}{2} \left( \frac{i}{a} \frac{\partial}{\partial \Phi(n_1)} \right)^2 + \frac{1}{2} \left( \frac{\hat{\Phi}(n_1+1) - \hat{\Phi}(n_1-1)}{2a} \right)^2 + \frac{m^2}{2} \hat{\Phi}(n_1)^2 + V(\hat{\Phi}(n_1)) \right]. \quad (3.28)$$

The unity can be written as

$$\mathbb{1} = \int_{-\infty}^{\infty} D[\Phi] |\Phi\rangle \langle \Phi|, \quad (3.29)$$

with the measure

$$D[\Phi] = \prod_{n_1} d\Phi(n_1). \quad (3.30)$$

Here we introduced eigenstates of Eq. (3.27), which in field representation are given by

$$\langle \Phi | \pi \rangle = \prod_{n_1} \sqrt{\frac{a}{2\pi}} e^{ia\Phi(n_1)\pi(n_1)}. \quad (3.31)$$

The steps for obtaining the Euclidean action for a scalar field theory will not be presented, but the idea is the same as in Section 3.3. First the matrix elements of  $\exp(-t\hat{H})$  are computed for the free case, which are then used for infinitesimal time steps in the Trotter formula.

The final theory lives on a 2-d lattice  $\Lambda_2$  with  $N^2$  lattice points. For our fields  $\Phi(\mathbf{x})$  and  $\pi(\mathbf{x})$  this corresponds to the change of  $\Phi(\mathbf{x}) \rightarrow \Phi(n_1, n_2)$  and  $\pi(\mathbf{x}) \rightarrow \pi(n_1, n_2)$ . Or in a more compact notation

$$\begin{aligned} \Phi(\mathbf{x}) &\rightarrow \Phi(\mathbf{n}), \\ \pi(\mathbf{x}) &\rightarrow \pi(\mathbf{n}), \end{aligned} \quad (3.32)$$

with the vector  $\mathbf{n} = (n_1, n_2)$ . The correlation function becomes

$$\langle O_2(t) O_1(0) \rangle = \frac{1}{Z_T} \int D[\Phi] e^{-S_E[\Phi]} O_2[\Phi(., n_t)] O_1[\Phi(., 0)], \quad (3.33)$$

where  $a \cdot n_t = t$  and with the Euclidean action given by

$$S_E[\Phi] = a^2 \sum_{\mathbf{n} \in \Lambda_2} \left[ \frac{1}{2} \sum_{j=1}^2 \left( \frac{\Phi(\mathbf{n} + \hat{j}) - \Phi(\mathbf{n} - \hat{j})}{2a} \right)^2 + \frac{m^2}{2} \Phi(\mathbf{n})^2 + V(\Phi(\mathbf{n})) \right]. \quad (3.34)$$

The action is now a 2-dimensional sum over the 2-d lattice  $\Lambda_2$ . The integral over all field configurations is mathematically well defined and the measure is a product measure,

$$D[\Phi] = \prod_{\mathbf{n} \in \Lambda_2} d\Phi(\mathbf{n}) . \quad (3.35)$$

Similar steps can be used for finding the lattice formulation of field theories with fermions. In this work we will not repeat those steps, but only present the final form of the lattice theory for the Gross-Neveu model analysed here.



# Chapter 4

## Wilson fermions

In the last section we have shown how to apply the discretisation to our system and obtained the lattice formulation. As will be seen, this formulation is still not the one we are using in the end, because it suffers from some lattice induced problems, the so-called *doublers*. To remove the doublers we will derive the *Wilson fermion action* which is the final form of the action we are going to work with.

Additionally we will discuss how to deal with fermions which require Fermi statistics. This can be implemented by using anti-commuting numbers for the quark fields, so-called *Grassman numbers*. The key formulas for calculating with Grassmann numbers are given in Sec. 4.2.

### 4.1 The lattice Gross-Neveu action

When we apply the discretisation steps of Chapter 3 we can write the lattice action as

$$S[\bar{\psi}, \psi, \Phi] = a^2 \sum_{\mathbf{n} \in \Lambda} \bar{\psi}(\mathbf{n}) \left[ \sum_{\mu=1}^2 \gamma_{\mu} \frac{\psi(\mathbf{n} + \hat{\mu}) - \psi(\mathbf{n} - \hat{\mu})}{2a} + m \psi(\mathbf{n}) + \sqrt{g} \Phi(\mathbf{n}) \psi(\mathbf{n}) \right] + \frac{1}{2} \Phi^2(\mathbf{n}) . \quad (4.1)$$

We can split the action in a fermionic and a scalar part  $S = S_F + S_S$ . Since the fermion action is bilinear in  $\bar{\psi}$  and  $\psi$ , we find the following form

$$S_F[\bar{\psi}, \psi, \Phi] = a^2 \sum_{\mathbf{n}, \mathbf{m} \in \Lambda} \bar{\psi}(\mathbf{n})_{\alpha} M(\mathbf{n}, \mathbf{m})_{\alpha\beta} \psi(\mathbf{m})_{\beta} , \quad (4.2)$$

$$S_S[\Phi] = \frac{1}{2} \sum_{\mathbf{n} \in \Lambda} \Phi^2(\mathbf{n}) . \quad (4.3)$$

We sum over  $\alpha$  and  $\beta$ , i.e., we use Einstein's summation convention. The Dirac operator  $M$  is given by

$$M(\mathbf{n}, \mathbf{m})_{\alpha\beta} = [ m + \sqrt{g} \Phi(\mathbf{n}) ] \delta_{\mathbf{n}, \mathbf{m}} \delta_{\alpha, \beta} - \sum_{\mu=1}^2 (\gamma_{\mu})_{\alpha\beta} \frac{\delta_{\mathbf{n}+\hat{\mu}, \mathbf{m}} - \delta_{\mathbf{n}-\hat{\mu}, \mathbf{m}}}{2a} . \quad (4.4)$$

In order to keep the notation simple the Dirac indices  $\alpha, \beta$  will be suppressed in the following.

### The doubling problem

Here we discuss Wilson's action and give reason for introducing it. First we apply a Fourier transformation to our Dirac matrix  $M(\mathbf{n}, \mathbf{m})$  for the free case  $g = 0$ . The definitions of Fourier transformation are given in Appendix A. We find

$$\begin{aligned} \text{FT}[M(\mathbf{n}, \mathbf{m})] &= \frac{1}{V} a^2 \sum_{\mathbf{n}, \mathbf{m} \in \Lambda} e^{-i\mathbf{p} \cdot \mathbf{n}a} M(\mathbf{n}, \mathbf{m}) e^{i\mathbf{q} \cdot \mathbf{m}a} \\ &= \frac{1}{V} a^2 \sum_{\mathbf{n} \in \Lambda} e^{-i(\mathbf{p}-\mathbf{q}) \cdot \mathbf{n}a} \left( \sum_{\mu=1}^2 \gamma_{\mu} \frac{e^{iq_{\mu}a} - e^{-iq_{\mu}a}}{2a} + m\mathbf{1} \right) \\ &= a^2 \delta(\mathbf{p} - \mathbf{q}) \hat{M}(\mathbf{p}) , \end{aligned} \quad (4.5)$$

with

$$\hat{M}(\mathbf{p}) = m + \frac{i}{a} \sum_{\mu=1}^2 \gamma_{\mu} \sin p_{\mu}a . \quad (4.6)$$

As one can see, the Fourier-transform is diagonal in momentum space. We want to compute the inverse operator in real space, the so-called *quark propagator*,  $M^{-1}(\mathbf{n}, \mathbf{m})$ . So we simply need to calculate the inverse of  $\hat{M}(\mathbf{p})$  and then apply a Fourier transformation back to real space. The inverse has the form

$$\hat{M}^{-1}(\mathbf{p}) = \frac{m - ia^{-1} \sum_{\mu} \gamma_{\mu} \sin p_{\mu}a}{m^2 + a^{-2} \sum_{\mu} \sin^2 p_{\mu}a} , \quad (4.7)$$

as can be seen from the identity:

$$[a + i b_{\mu} \gamma_{\mu}]^{-1} = \frac{a - i b_{\mu} \gamma_{\mu}}{a^2 + b^2} . \quad (4.8)$$

The quark propagator governs the behaviour of functions. So it is important to analyse the propagator, which is simplest in momentum space. We set the mass  $m = 0$ , and see that the propagator has the correct continuum limit,

$$\hat{M}^{-1}(\mathbf{p})|_{m=0} = \frac{-ia^{-1} \sum_{\mu} \gamma_{\mu} \sin p_{\mu} a}{a^{-2} \sum_{\mu} \sin^2 p_{\mu} a} \xrightarrow{a \rightarrow 0} \frac{-i \sum_{\mu} \gamma_{\mu} p_{\mu}}{p^2}. \quad (4.9)$$

In the continuum, the propagator has a pole for the massless case at

$$\mathbf{p} = (0, 0), \quad (4.10)$$

but on the lattice this is different. There exist additional poles at

$$\mathbf{p} = \left(\frac{\pi}{a}, 0\right), \quad \mathbf{p} = \left(0, \frac{\pi}{a}\right), \quad \mathbf{p} = \left(\frac{\pi}{a}, \frac{\pi}{a}\right). \quad (4.11)$$

These poles are the so-called *doublers*, which have to be removed in a proper lattice formulation.

### The Wilson term

In order to get rid of the doublers Wilson suggested to add an extra term to the momentum space propagator (4.6) [26]. The propagator then reads

$$\hat{M}(\mathbf{p}) = m + \frac{i}{a} \sum_{\mu=1}^2 \gamma_{\mu} \sin p_{\mu} a + \frac{1}{a} \sum_{\mu=1}^2 (1 - \cos p_{\mu} a). \quad (4.12)$$

This extra *Wilson term* vanishes for  $p_{\mu} = 0$ , but for each  $p_{\mu} = \pi/a$  it provides an extra contribution  $2l/a$ , where  $l$  is the number of momentum components with  $p_{\mu} = \pi/a$ . In the continuum limit  $a \rightarrow 0$ , this term can be understood as an additional mass term which becomes infinitely heavy, and so the doublers decouple from the theory. The form of the Wilson term in real space can be found by an inverse Fourier transformation and reads

$$-\frac{a}{2} \sum_{\mu=1}^2 \frac{\delta_{\mathbf{n}+\hat{\mu}, \mathbf{m}} - 2\delta_{\mathbf{n}, \mathbf{m}} + \delta_{\mathbf{n}-\hat{\mu}, \mathbf{m}}}{a^2} \xrightarrow{a \rightarrow 0} -\frac{a}{2} \partial_{\mu} \partial_{\mu}. \quad (4.13)$$

The final form of the kernel of the fermion action then is

$$M(\mathbf{n}, \mathbf{m}) = [2 + m + \sqrt{g} \Phi(\mathbf{n})] \delta_{\mathbf{n}, \mathbf{m}} - \sum_{\mu=\pm 1}^{\pm 2} \Gamma_{\pm \mu} \delta_{\mathbf{n}+\hat{\mu}, \mathbf{m}}, \quad (4.14)$$

with

$$\Gamma_{\pm\mu} = \frac{1}{2}(\mathbb{1} \mp \gamma_\mu) . \quad (4.15)$$

This is the form of the Dirac matrix which we are going to implement in our computer program, and with the inverse of it, we are going to compute our correlation functions according to Wick's theorem. The Wilson term breaks chiral symmetry explicitly even for the massless case  $m = 0$ . The pioneers for the Gross-Neveu model with Wilson fermions were Aoki and Higashijima [27].

## 4.2 Key formulas for fermions on the lattice

In the last section we have derived the action of our model. What we have missed is the discussion of how to deal with fermions. Fermions have to satisfy Fermi statistics. That requires that they are anti-symmetric under pair permutation. If we interchange two fermions with each other, we acquire a minus sign. Thus, one can say fermions behave like anti-commuting numbers, for any combination of the indices  $f, f', n, n', \alpha, \alpha', a, a'$ , where  $f$  stands for the flavor index,  $n$  for a lattice site,  $\alpha$  for the Dirac index and  $a$  for the color index, which we add here in order to get a general knowledge of Fermi statistics.

$$\psi^{(f)}(n)_{\alpha,a} \psi^{(f')}(n')_{\alpha',a'} = -\psi^{(f')}(n')_{\alpha',a'} \psi^{(f)}(n)_{\alpha,a} . \quad (4.16)$$

We also demand

$$\bar{\psi}^{(f)}(n)_{\alpha,a} \bar{\psi}^{(f')}(n')_{\alpha',a'} = -\bar{\psi}^{(f')}(n')_{\alpha',a'} \bar{\psi}^{(f)}(n)_{\alpha,a} , \quad (4.17)$$

$$\psi^{(f)}(n)_{\alpha,a} \bar{\psi}^{(f')}(n')_{\alpha',a'} = -\bar{\psi}^{(f')}(n')_{\alpha',a'} \psi^{(f)}(n)_{\alpha,a} . \quad (4.18)$$

### Grassmann numbers

We need to know the calculation rules for Grassmann numbers in order to work with them. Consider a set of Grassmann numbers  $\eta_i$ ,  $i = 1, \dots, N$ . They obey

$$\eta_i \eta_j = -\eta_j \eta_i . \quad (4.19)$$

To fulfill this equation, the Grassmann numbers have to be nilpotent ( $\eta_i^2 = 0$ ). So the power series ends after a finite number of terms. Thus the only relevant class of functions are polynomials,

$$A = a + \sum_i a_i \eta_i + \sum_{i<j} a_{ij} \eta_i \eta_j + \sum_{i<j<k} a_{ijk} \eta_i \eta_j \eta_k + \dots + a_{12\dots N} \eta_1 \eta_2 \dots \eta_N . \quad (4.20)$$

For derivatives the following rules exist:

$$\frac{\partial}{\partial \eta_i} 1 = 0, \quad \frac{\partial}{\partial \eta_i} \eta_i = 1, \quad \frac{\partial}{\partial \eta_i} \frac{\partial}{\partial \eta_j} = -\frac{\partial}{\partial \eta_j} \frac{\partial}{\partial \eta_i}, \quad \frac{\partial}{\partial \eta_i} \eta_j = -\eta_j \frac{\partial}{\partial \eta_i}. \quad (4.21)$$

In addition to differentiation, we need to give the calculation rules for integration,

$$\int d^N \eta \frac{\partial}{\partial \eta_i} A = 0. \quad (4.22)$$

The normalisation

$$\int d^N \eta \eta_1 \eta_2 \dots \eta_N = 1, \quad \text{implies} \quad \int d^N A = a_{12\dots N}. \quad (4.23)$$

The measure  $d^N \eta$  is a product

$$d^N \eta = d\eta_N d\eta_{N-1} \dots d\eta_1, \quad (4.24)$$

which we transform under a linear change of variables given by

$$\eta'_i = \sum_{j=1}^N M_{ij} \eta_j. \quad (4.25)$$

$M$  is a complex  $N \times N$  matrix. If we apply this change we get

$$\begin{aligned} \int d^N \eta \eta_1 \eta_2 \dots \eta_N &= \int d^N \eta' \eta'_1 \eta'_2 \dots \eta'_N = \int d^N \eta' \sum_{i_1, \dots, i_N} M_{1i_1} \dots M_{Ni_N} \eta_{i_1} \dots \eta_{i_N} \\ &= \int d^N \eta' \sum_{i_1, \dots, i_N} M_{1i_1} \dots M_{Ni_N} \epsilon_{i_1 i_2 \dots i_N} \eta_1 \dots \eta_N = \det[M] \int d^N \eta' \eta_1 \dots \eta_N. \end{aligned} \quad (4.26)$$

So the transformation property of the measure in the Grassmann integration is

$$d^N \eta = \det[M] d^N \eta'. \quad (4.27)$$

At the end we want to conclude with the definition of the result for a Gaussian integral with Grassmann numbers. We have a Grassmann algebra with  $2N$  generators  $\eta_i, \bar{\eta}_i, i = 1, \dots, N$ , which fulfill the above mentioned rules. The so-called *Matthews-Salam formula* gives

$$Z_F = \int d\eta_N d\bar{\eta}_N \dots d\eta_1 d\bar{\eta}_1 \exp \left( \sum_{i,j=1}^N \bar{\eta}_i M_{ij} \eta_j \right) = \det[M], \quad (4.28)$$

where  $M$  is again a complex  $N \times N$  matrix. The result can be proven by using the transformation property of Eq. (4.27).

### 4.3 The free case $g = 0$

In order to compute the correlation matrix of Eq. (3.2), we need to know the inverse of the Dirac matrix. The reason for that will be explained in Sec. 6.1.

In the free case the coupling constant  $g$  is equal to zero. This case is very important, because it allows to check our complex computer program by a comparison of the numerical results with exact results from Fourier transformation. Hence, the free case provides us with an analytical expression of the correlation function.

#### Derivation of the inverse Dirac operator

The Dirac operator for  $g = 0$  has the form

$$M(\mathbf{n}, \mathbf{m}) = (2 + m) \delta_{\mathbf{n}, \mathbf{m}} - \sum_{\mu=\pm 1}^{\pm 2} \Gamma_{\pm\mu} \delta_{\mathbf{n}+\hat{\mu}, \mathbf{m}} . \quad (4.29)$$

We apply Fourier transformation and obtain

$$\text{FT}[M(\mathbf{n}, \mathbf{m})] = \tilde{M}(\mathbf{p}, \mathbf{q}) = \frac{1}{V} \sum_{\mathbf{n}, \mathbf{m}} e^{-i\mathbf{p}\mathbf{n}} M(\mathbf{n}, \mathbf{m}) e^{i\mathbf{q}\mathbf{m}} . \quad (4.30)$$

The calculation works the same way as in Eq. (4.5), where the doubling problem was discussed. For notational convenience we suppress the factor  $a$ , the lattice spacing. As before we get

$$\tilde{M}(\mathbf{p}, \mathbf{q}) = \delta(\mathbf{p} - \mathbf{q}) \hat{M}(\mathbf{p}) , \quad (4.31)$$

where

$$\hat{M}(\mathbf{p}) = N(\mathbf{p}) + i \sum_{\mu} \gamma_{\mu} \sin p_{\mu} . \quad (4.32)$$

We introduce the abbreviations

$$N(\mathbf{p}) = 2 + m - \sum_{\mu=1}^2 \cos p_{\mu} \quad (4.33)$$

and

$$D(\mathbf{p}) = N^2(\mathbf{p}) + \sum_{\mu=1}^2 \sin^2 p_{\mu} . \quad (4.34)$$

The operator  $\tilde{M}$  is diagonal in momentum space, so it is easy to invert it. It follows

$$\tilde{M}^{-1}(\mathbf{p}, \mathbf{q}) = \delta(\mathbf{p} - \mathbf{q}) \hat{M}^{-1}(\mathbf{p}) , \quad (4.35)$$

with

$$\hat{M}^{-1}(\mathbf{p}) = \frac{1}{D(\mathbf{p})} [N(\mathbf{p}) - i \sum_{\mu} \gamma_{\mu} \sin p_{\mu}] . \quad (4.36)$$

If we Fourier transform back to real space we find our final expression for the quark propagator in the free case,

$$M^{-1}(\mathbf{n}, \mathbf{m}) = \frac{1}{V} \sum_{\mathbf{p}} e^{i\mathbf{p}(\mathbf{n}-\mathbf{m})} \hat{M}^{-1}(\mathbf{p}) . \quad (4.37)$$

In our program the inverse of the Dirac matrix is calculated using the *LAPACK* routines [28]. With (4.37) we are able to check if we have implemented our matrix correctly for the case  $g = 0$ . Furthermore we can insert the analytical expression in our correlation matrix and calculate each matrix element exactly in the free case. Thus we can also check the correctness of parts of the analysis.

## 4.4 Spectrum of the Dirac operator

The Dirac operator of Eq. (4.14) has a very characteristic spectrum of the eigenvalues. We want to analyse this spectrum as a check for our programmed Dirac matrix. The eigenvalue equation is given by

$$M v_{\lambda} = \lambda v_{\lambda} , \quad (4.38)$$

where  $\lambda$  is the eigenvalue of the Dirac matrix  $M$  and  $v_{\lambda}$  the corresponding eigenvector. The Dirac operator is  $\gamma_5$ -hermitian, which means it obeys the following equation,

$$\gamma_5 M \gamma_5 = M^{\dagger} . \quad (4.39)$$

This requirement has an interesting consequence for the spectrum. The characteristic polynomial  $P(\lambda)$  reads

$$\begin{aligned} P(\lambda) &= \det[M - \lambda \mathbf{1}] = \det[\gamma_5^2 (M - \lambda \mathbf{1})] = \det[\gamma_5 (M - \lambda \mathbf{1}) \gamma_5] \\ &= \det[M^{\dagger} - \lambda \mathbf{1}] = \det[M - \lambda^* \mathbf{1}]^* = P(\lambda^*)^* . \end{aligned} \quad (4.40)$$

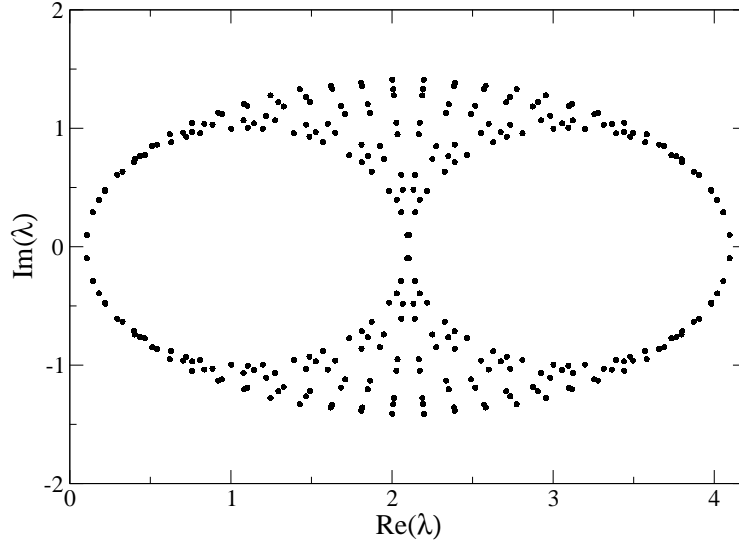


**Figure 4.1:** Eigenvalue spectrum of the Dirac matrix  $M$  for a  $16 \times 32$  lattice, with the coupling constant  $g = 0$ , the bare mass  $m = 0.1$  and  $N_f = 2$ .

We inserted  $\gamma_5^2 = \mathbb{1}$  and applied the  $\gamma_5$ -hermiticity. As known, the eigenvalues are the zeros of  $P(\lambda)$ , and due to Eq. (4.40), if  $\lambda$  is a zero, so is  $\lambda^*$ . Thus the eigenvalues come in complex conjugate pairs.

Another implication of Eq. (4.39) concerns the  $\gamma_5$  matrix element of the eigenvectors. We find

$$\lambda v_\lambda^\dagger \gamma_5 v_\lambda = v_\lambda^\dagger \gamma_5 M v_\lambda = v_\lambda^\dagger M^\dagger \gamma_5 v_\lambda = (M v_\lambda)^\dagger \gamma_5 v_\lambda = \lambda^* v_\lambda^\dagger \gamma_5 v_\lambda, \quad (4.41)$$

and thus  $\text{Im}(\lambda) (v_\lambda^\dagger \gamma_5 v_\lambda) = 0$ . Hence either  $\text{Im}(\lambda) = 0$ , and then it is possible for the  $\gamma_5$  sandwich to be  $v_\lambda^\dagger \gamma_5 v_\lambda \neq 0$ , or  $\text{Im}(\lambda) \neq 0$  and the sandwich vanishes.

In Fig. 4.1 we show the eigenvalues of the Dirac matrix for the coupling constant  $g = 0$  and the mass  $m = 0.1$ . As one can see the eigenvalues come in complex conjugate pairs, and the spectrum forms an ellipsoid with a rather sharp outline. For  $m = 0$  the spectrum would start exactly at the origin. Increasing the coupling constant  $g$ , the spectrum of the ellipsoid will get shifted towards negative values as can be seen in Fig. 4.2 ( $N_f = 2$ ), and the contour of the ellipsoid becomes blurred.

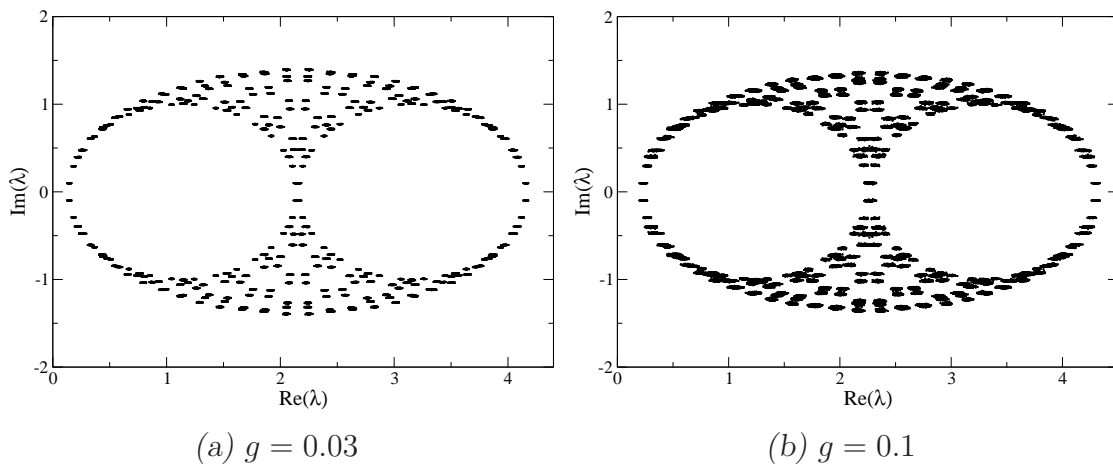


**Figure 4.2:** The eigenvalue spectra of the Dirac operator near the origin is plotted for the mass  $m = 0.1$  and a  $16 \times 32$  lattice for  $N_f = 2$ , for 100 configurations in (a), and 200 configurations in (b).

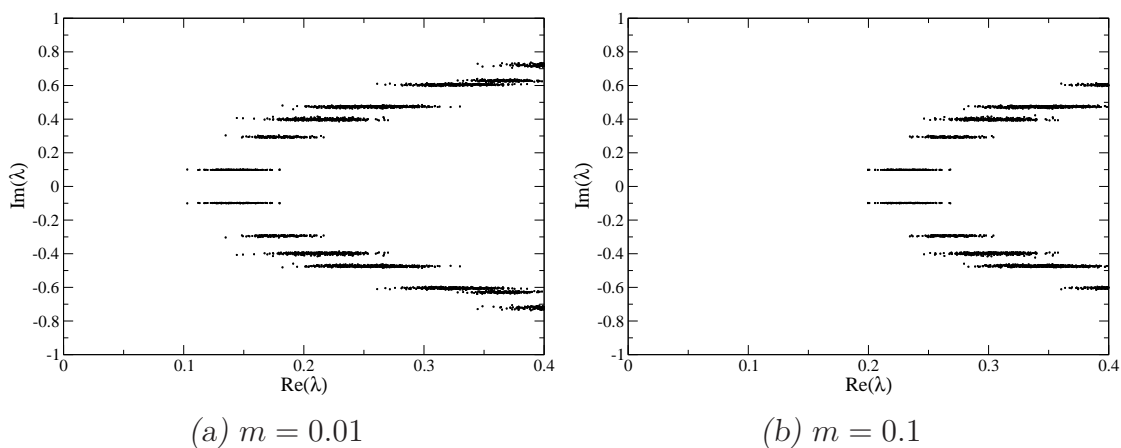


**Figure 4.3:** This plot shows the shift of the edge of the Dirac spectrum when adding a mass term  $m$  ( $N_f = 2$ ).

By varying now the mass term  $m$ , it is possible to shift the whole spectrum back to the origin. For  $g = 0$  the spectrum starts in the origin, for increasing  $g$  a shift takes place into the negative direction. Increasing  $m$ , we can now control the spectrum and bring it back to the origin. This can be seen in Fig. 4.3 by

a comparison of two different masses for one coupling constant  $g = 0.1$  and a  $16 \times 32$  lattice, each for 200 configurations at  $N_f = 2$ .

If the edge of the spectrum touches the origin we obtain massless fermions. On the other hand if the spectrum is shifted to the right, the distance of the edge of the spectrum to the origin gives the bare fermion mass.

# Chapter 5

## Numerical simulations

In this chapter we will first introduce the basic numerical method to generate the configurations for the scalar field  $\Phi$ , the Monte-Carlo algorithm. With this algorithm quenched fermions can be simulated, where the fermion determinant is set  $\det(M[\Phi]) = 1$ . Another approach which can be applied is the so-called reweighting technique, see Paragraph 5.1.3. In Sec. 5.2 we will introduce the Hybrid-Monte Carlo (HMC) method, where dynamical fermions can be simulated. This algorithm is much more complex in general. Our configurations will always be simulated with the HMC method.

### 5.1 Monte-Carlo simulations on the lattice

The name *Monte Carlo*, known from the casinos in Monte Carlo, seems to already tell everything. It gives us the hint that something happens randomly, by chance. Monte Carlo methods are a widely used class of computational algorithms for simulating the behaviour of various physical and mathematical systems, and for other computations. They are distinguished from other simulation methods by being stochastic, usually by using random numbers. It is one of the main tools in the numerical calculations of this diploma thesis.

#### 5.1.1 Central idea of Monte-Carlo simulations

In order to give a motivation for using Monte-Carlo techniques, a short but hopefully very plausible example will be given. Consider the Ising model, which is a

model for simulating a ferromagnet, in 2 dimensions for a  $100 \times 100$  lattice. Each lattice site is occupied with one of the two spin values  $+1$  or  $-1$ . They represent magnets, pointing up or down. In this system exist  $2^{100 \times 100}$  configurations. For calculating the partition function we have to take the sum over all possible configurations  $C$ ,

$$Z = \sum_C P(C) , \quad (5.1)$$

with  $P(C)$  being the probability for one configuration. No computer can ever complete such a calculation, because it takes too much computer time. A Monte-Carlo simulation replaces the sum over all configurations by a representative, but smaller set. We can get this sample by two different ways.

*Simple sampling*, where each configuration is chosen randomly and entirely by chance, such that each configuration has the same probability of being chosen at any stage during the sampling process.

*Importance sampling*, where a probability factor is included in the choice of the configurations, because some configurations have more impact or are more likely. If these "important" values are emphasised by sampling more frequently, then the estimator variance can be reduced.

For importance sampling the expectation value of an observable is given by

$$\langle O \rangle = \lim_{N \rightarrow \infty} \frac{1}{N} \sum_{n=1}^N O(C_n) , \quad (5.2)$$

with  $C_n$ , being the  $n^{\text{th}}$  configuration. The statistical error of the result is proportional to  $1/\sqrt{N}$ . The exact result is obtained for  $N \rightarrow \infty$ .

### 5.1.2 Markov chain

We want to find the configuration  $C_n$ . The idea is to start from some arbitrary configuration  $C_0$  and construct a sequence of configurations, with a certain probability distribution. This sequence is called *Markov chain*, which leads to

$$C_0 \longrightarrow C_1 \longrightarrow C_2 \longrightarrow C_3 \longrightarrow \dots . \quad (5.3)$$

The transition from  $C_i$  to  $C_{i+1}$  is called an *update*. Later in Sec. 5.3, an accept/reject step will be included, which leads to the *Metropolis algorithm*. A

Markov process is characterised by transition amplitudes  $T$ , between only two points in configuration space. Its definition is

$$T(C'|C) = W(C^{(n)} = C' | C^{(n-1)} = C) . \quad (5.4)$$

The transition probability has to fulfill the two equations

$$0 \leq T(C'|C) \leq 1 , \quad (5.5)$$

$$\sum_{C'} T(C'|C) = 1 . \quad (5.6)$$

The probability to hop into a configuration  $C_n$ , has to be the same as hopping out of it. So, the corresponding equation which satisfies this statement is the balance equation, which reads

$$\sum_C T(C'|C) P(C) = \sum_C T(C|C') P(C') . \quad (5.7)$$

A solution of (5.7) is the requirement of

$$T(C'|C) P(C) = T(C|C') P(C') , \quad (5.8)$$

the so-called *detailed balance* condition. The Markov chain has to be ergodic, i.e., every configuration in the configuration space can be reached in a finite number of steps.

### 5.1.3 The reweighting algorithm for the Gross-Neveu model

For this case the Monte-Carlo method becomes pretty simple. Each configuration depends just on the scalar field  $\Phi$ . One generates the configurations according to the Gaussian distribution

$$P \propto \frac{1}{\sqrt{2\pi}} e^{-\Phi^2/2} . \quad (5.9)$$

The approximation of the expectation value of an observable ( $N_f = 1$ ) is then given by

$$\langle O \rangle_\Phi = \frac{\sum_{i=1}^N \det(M[\Phi])_i O[M[\Phi], \Phi]_i}{\sum_{i=1}^N \det(M[\Phi])_i} . \quad (5.10)$$

This is a re-weighting of the distributed scalar fields with the fermion determinant, which means we also have to compute the  $\det(M[\Phi])$ . Later, in the analysis we have to reintroduce the determinant in the calculations of the correlation matrix. So the evaluation becomes a little bit more difficult than just summing up all  $N$  measurements.

## 5.2 Techniques for dynamical Fermions

The strategy of Sec. 5.1 included the fermion determinant with a re-weighting technique, and did not take into account the fermion dynamics in the algorithm. However, the calculation of dynamical fermions is much more challenging, than a quenched ( $\det M[\Phi] = 1$ ) calculation, or the above mentioned reweighting technique. The problem is that the fermion determinant is a functional of the gauge field (in QCD), and so has to be computed new for every configuration. Usually the Dirac operator is a huge matrix with  $N = 12|\Lambda|$  rows and columns, where  $|\Lambda|$  is the number of lattice points, and the factor 12 is the product of color and Dirac indices (for 4-d QCD). This means high computational costs! Furthermore the determinant is very small for most configurations generated with only the scalar action (GN model). Thus one should include the determinant in the generation of the  $\Phi$ . The methods discussed now implement this strategy.

### Pseudofermion fields

There exists an equivalence between fermionic and bosonic Gaussian integrals. This similarity has led to the introduction of the so-called *pseudofermions*, which are bosons with the same number of degrees of freedoms as the fermionic variables. The central idea is to replace the fermion determinant by a Gaussian integral of a bosonic field. We use again  $\gamma_5$ -hermiticity and obtain

$$\begin{aligned} \det[M]^2 &= \det[M] \det[M] \det[\gamma_5^2] = \det[M] \det[\gamma_5] \det[M] \det[\gamma_5] \\ &= \det[M \ M^\dagger] = \pi^{-N} \int D[\alpha_R] D[\alpha_I] e^{-\alpha^\dagger (M \ M^\dagger)^{-1} \alpha} . \end{aligned} \quad (5.11)$$

Because the fermion determinant can be written as an integral over the Grassman

variables, see (4.28), it follows

$$\int D[\psi] D[\bar{\psi}] e^{-\bar{\psi}_1 M \psi_1 - \bar{\psi}_2 M \psi_2} = \pi^{-N} \int D[\alpha_R] D[\alpha_I] e^{-\alpha^\dagger (M M^\dagger)^{-1} \alpha} . \quad (5.12)$$

We here have assumed two mass-degenerate flavors. The number of fermions has to be even because we want to guarantee positivity in order to have convergence for the integral. The problem is that the fermion determinant is highly non local. This means if we change the scalar fields  $\Phi$  at a single point, the change of  $(M[\Phi]M^\dagger[\Phi])^{-1}$  may be large and the change of the action is too big to be accepted. In the next step we explain how to get rid of this problem.

## 5.3 Hybrid Monte-Carlo algorithm

If we update a bosonic field, in our case the scalar field  $\Phi$ , this step has two parts. In the first one, a reasonable suggestion for the change has to be made. This leads to a selection probability factor  $T_0(\Phi'|\Phi)$ . The second step is a Metropolis *accept/reject* step as announced in Sec. 5.1.2, with the acceptance probability  $T_A(\Phi'|\Phi)$ . This leads to the complete transition probability

$$T(\Phi'|\Phi) = T_A(\Phi'|\Phi) T_0(\Phi'|\Phi) . \quad (5.13)$$

But first it has to be discussed how to come to a configuration  $\Phi'$ .

### 5.3.1 The molecular dynamics leapfrog evolution

The basic idea is to introduce for the scalar field  $\Phi$  a corresponding momentum  $P$ , (for simplicity we suppress the lattice index). We write the vacuum expectation value of an observable as

$$\begin{aligned} \langle O \rangle_\Phi &= \frac{\int D[\Phi] \exp(-S[\Phi]) O[\Phi]}{\int D[\Phi] \exp(-S[\Phi])} \\ &= \frac{\int D[\Phi] D[P] \exp(-\frac{P^2}{2} - S[\Phi]) O[\Phi]}{\int D[\Phi] D[P] \exp(-\frac{P^2}{2} - S[\Phi])} = \langle O \rangle_{\Phi, P} . \end{aligned} \quad (5.14)$$

The Gaussian integral over  $P$  can be solved, so that the two factors in the denominator and the numerator cancel. The two forms are equivalent. But now

the new form represents a microcanonical ensemble with the Hamiltonian of a classical system,

$$H[\Phi, P] \equiv \frac{1}{2}P^2 + S[\Phi] . \quad (5.15)$$

The advantage here is that if we evolve the Hamiltonian using the canonical equations, the energy stays constant for all times, and thus the new configurations  $\Phi'$  and  $P'$  are always accepted,

$$H[\Phi, P] = H[\Phi', P'] . \quad (5.16)$$

In reality numerical errors occur in the evolution, so that the configurations  $(\Phi, P)$  do not all lie on the same hypersurface of constant energy.

The classical equations of motion are

$$\begin{aligned} \dot{P} &= -\frac{\partial H}{\partial \Phi} = -\frac{\partial S}{\partial \Phi} , \\ \dot{\Phi} &= -\frac{\partial H}{\partial P} . \end{aligned} \quad (5.17)$$

The *leapfrog evolution* consists of evolving  $\Phi$  in  $n$  steps, with stepsize  $\epsilon$ , and the conjugate momenta by starting with a half-step  $\epsilon/2$ , and  $(n - 1)$  full steps, and a final half step. The prescription for the evolution is as follows:

$$\begin{aligned} 1 : P^{(n)}(x) &\longrightarrow P^{(n+\frac{1}{2})}(x) = P^{(n)}(x) - f[\Phi^{(n)}](x) \frac{\epsilon}{2} \\ 2 : \Phi^{(n)}(x) &\longrightarrow \Phi^{(n+1)}(x) = \Phi^{(n)}(x) + P^{(n+\frac{1}{2})}(x)\epsilon \\ 3 : P^{(n+\frac{1}{2})}(x) &\longrightarrow P^{(n+1)}(x) = P^{(n+\frac{1}{2})}(x) - f[\Phi^{(n+1)}](x) \frac{\epsilon}{2} , \end{aligned} \quad (5.18)$$

where  $f[\Phi](x) = -\dot{P}(x)$ .

### 5.3.2 Implementing HMC for the Gross-Neveu model

For the following discussion we assume two dynamical flavors of quarks. The scalar field  $\Phi$  and the pseudofermion fields  $\alpha$  are distributed with the Boltzman weight

$$\exp(-S[\Phi, \alpha]) , \quad S[\Phi, \alpha] = S[\Phi] - \alpha^\dagger (M M^\dagger)^{-1} \alpha . \quad (5.19)$$

The pseudofermion fields  $\alpha$  are updated by generating a complex vector  $\chi$ , and setting  $\alpha = M\chi$ .  $\chi$  is distributed according to the Gaussian distribution

$\exp(-\chi^\dagger \chi)$ . The expectation value of the observable including now the dynamical behaviour of the quarks is

$$\begin{aligned} \langle O \rangle &= \frac{\int D[\Phi] e^{-S[\Phi]} (\det M[\Phi])^{2n} O[\Phi]}{\int D[\Phi] e^{-S[\Phi]} (\det M[\Phi])^{2n}} \\ &\stackrel{n=1}{=} \frac{\int D[\Phi] D[\alpha] e^{-S[\Phi]} e^{-\alpha^\dagger (M M^\dagger)^{-1} \alpha} O[\Phi]}{\int D[\Phi] D[\alpha] e^{-S[\Phi]} e^{-\alpha^\dagger (M M^\dagger)^{-1} \alpha}}. \end{aligned} \quad (5.20)$$

The next step is the inclusion of the conjugate momenta  $P$  as in Eq. (5.14). For the evolution of  $P$  we need to know  $\dot{P}$ . It is given by

$$\begin{aligned} \dot{P}(x) &= -\frac{\partial}{\partial \Phi(x)} \left( \frac{1}{2} \sum_y \Phi^2(y) + \alpha^\dagger(y) (M[\Phi] M^\dagger[\Phi])^{-1} \alpha(y) \right) \\ &= -\Phi(x) + \alpha^\dagger(x) \left[ M^{\dagger^{-1}} M^{-1} \frac{\partial M}{\partial \Phi(x)} M^{-1} + M^{\dagger^{-1}} \frac{\partial M^\dagger}{\partial \Phi(x)} M^{\dagger^{-1}} M^{-1} \right] \alpha(x) \\ &= -\Phi(x) + v^\dagger \left[ M^{-1} \frac{\partial M}{\partial \Phi(x)} + \frac{\partial M^\dagger}{\partial \Phi(x)} M^{\dagger^{-1}} \right] v \\ &= -\Phi(x) + \sum_{y,z,w} v^\dagger(y) \left[ M^{-1}(y,z) \frac{\partial M(z,w)}{\partial \Phi(x)} + \frac{\partial M^\dagger(y,z)}{\partial \Phi(x)} M^{\dagger^{-1}}(z,w) \right] v(w) \\ &= -\Phi(x) + \sqrt{g} \sum_{y,z,w} v^\dagger(y) M^{-1}(y,z) \delta_{z,x} \delta_{w,x} v(w) \\ &\quad + \sqrt{g} \sum_{y,z,w} v^\dagger(y) \delta_{y,x} \delta_{z,x} M^{\dagger^{-1}}(z,w) v(w) \\ &= -\Phi(x) + \sqrt{g} \sum_y v^\dagger(y) M^{-1}(y,x) v(x) + \sqrt{g} \sum_w v^\dagger(x) M^{\dagger^{-1}}(x,w) v(w) \\ &= -\Phi(x) + 2\sqrt{g} \operatorname{Re} \sum_w v^\dagger(w) M^{\dagger^{-1}}(x,w) v(w) \\ &= -f[\Phi](x), \end{aligned} \quad (5.21)$$

where  $v = M[\Phi]^{-1} \alpha$  and  $\frac{\partial M(z,w)}{\partial \Phi(x)} = \sqrt{g} \mathbf{1} \delta_{x,z} \delta_{x,w}$ .

The complete HMC algorithm then becomes

1. Start, e.g., with  $\Phi = 0$  (coldstart).
2. Generate the pseudofermion field  $\alpha[\Phi]$ , with  $\alpha[\Phi] = M[\Phi] \chi$ .
3. Generate  $P$  according to the distribution  $P[P] = \exp(-\sum_x P(x)^2/2)$ .

4. Make a leapfrog evolution using Eq. (5.18), where  $f[\Phi^{(n)}]$  is given by Eq. (5.21). It is convenient to rewrite the leapfrog evolution.

The first half-step of  $P$  and full-step of  $\Phi$  is given by

$$\begin{aligned} P^{(\frac{1}{2})}(x) &= P^{(0)}(x) - f[\Phi^{(0)}](x)\frac{\epsilon}{2}, \\ \Phi^{(1)}(x) &= \Phi^{(0)}(x) + P^{(\frac{1}{2})}(x)\epsilon. \end{aligned} \quad (5.22)$$

The trick is that we now can start to recursively insert the steps. This evolution will be repeated  $n = 1, \dots, n_{\text{steps}} - 1$  times, with  $n_{\text{steps}}$  being the number of steps made for one trajectory,

$$\begin{aligned} P^{(n+\frac{1}{2})}(x) &= P^{(n-\frac{1}{2})}(x) - f[\Phi^{(n)}](x)\epsilon, \\ \Phi^{(n+1)}(x) &= \Phi^{(n)}(x) + P^{(n+\frac{1}{2})}(x)\epsilon. \end{aligned} \quad (5.23)$$

At the end there is one last half-step

$$P^{(n+1)}(x) = P^{(n+\frac{1}{2})}(x) - f[\Phi^{(n+1)}](x)\frac{\epsilon}{2}. \quad (5.24)$$

5. Do the Metropolis accept/reject step at the end of the trajectory:

The random number  $r$  is  $r \in [0, 1]$ . Compute  $\rho \in [0, \infty)$

$$\rho = \frac{\exp(-P'^2/2 - V[\Phi'])}{\exp(-P^2/2 - V[\Phi])}, \quad (5.25)$$

with

$$V[\Phi] = \frac{\Phi^2}{2} + \alpha^\dagger [M[\Phi]M^\dagger[\Phi]]^{-1} \alpha. \quad (5.26)$$

If  $r \leq \rho$  accept  $\Phi'$  and  $P'$  as the new configuration, else go back to step 2. and generate a new pseudofermion field  $\alpha$ .

For each trajectory the field  $\alpha$  depends on  $\Phi$ , i.e.,  $\alpha = \alpha[\Phi]$ .

For the actual calculation the scalar field  $\Phi$  has to be brought into equilibrium. After that, we can generate, starting from the equilibrium configuration, new configurations  $\Phi$ . At the end, we get a set of configurations  $\Phi$ , which we can use for computing the expectation values (5.2).

# Chapter 6

## Interpolators and their symmetries

In this work we want to compute the masses of ground and excited states. The first thing we have to do is to build particle interpolators  $O, O^\dagger$  for the correlation function. These interpolators annihilate and create the particle states we want to analyse.

A particle interpolator has the basic form

$$O(t) = \frac{1}{L_x} \sum_x \bar{\psi}(x, t) \Gamma \psi(x, t) . \quad (6.1)$$

$\Gamma$  is one of the Dirac matrices (Pauli matrices in  $2d$ ) and the sum over the spatial coordinate  $x$  projects to zero momentum (see below).

The correlation functions we want to compute are

$$C_{ij}(t) = \langle O_i(t) O_j(0)^\dagger \rangle - \langle O_i(t) \rangle \langle O_j(0)^\dagger \rangle . \quad (6.2)$$

There are many possible interpolators  $O_i$  we can construct, since there are many combinations of quantum numbers such as spin, parity, charge conjugation, flavor content, etc. In the  $1 + 1$ -dimensional Gross-Neveu model we obtain just two different types of interpolators. One type with positive parity and one set with negative parity. A list of all used interpolators will be given below. The symmetry transformations for some example interpolators are given in Section 6.3.

In order to fill the correlation matrix with its entries we have to compute every single matrix element. For this, we apply *Wick's theorem*.

## 6.1 Wick's theorem

With this theorem [29] it is possible to calculate expectation values of the fermionic spinor fields, using the fact that fermion fields are anti-commuting *Grassmann numbers*. The formula reads

$$\begin{aligned} \langle \eta_{i_1} \bar{\eta}_{j_1} \dots \eta_{i_n} \bar{\eta}_{j_n} \rangle_F &= \frac{1}{Z_F} \int \prod_{k=1}^N d\eta_k d\bar{\eta}_k \eta_{i_1} \bar{\eta}_{j_1} \dots \eta_{i_n} \bar{\eta}_{j_n} \exp \left( \sum_{l,m=1}^N \bar{\eta}_l M_{lm} \eta_m \right) \\ &= (-1)^n \sum_{P(1,2,\dots,n)} \text{sign}(P) (M^{-1})_{i_1 j_{P_1}} (M^{-1})_{i_2 j_{P_2}} \dots (M^{-1})_{i_n j_{P_n}} . \end{aligned} \quad (6.3)$$

For better understanding we give an example of the application of Wick's theorem. We compute the expectation value

$$\langle O_1(t) O_2(0)^\dagger \rangle , \quad (6.4)$$

with

$$O_1(t) = \frac{1}{L_x} \sum_x \langle \bar{\psi}_\alpha(x, t) (\gamma_5)_{\alpha\beta} \psi_\beta(x, t) \rangle , \quad (6.5)$$

and

$$O_2(0)^\dagger = \frac{1}{L_y} \sum_y \langle \bar{\psi}_\gamma(y, 0) (\gamma_5)_{\gamma\delta} \psi_\delta(y, 0) \rangle^\dagger . \quad (6.6)$$

Then Eq. (6.3) turns into

$$\begin{aligned} & \frac{1}{L_x} \frac{1}{L_y} \sum_{x,y} \langle (\bar{\psi}_\alpha(x, t) (\gamma_5)_{\alpha\beta} \psi_\beta(x, t)) (\bar{\psi}_\gamma(y, 0) (\gamma_5)_{\gamma\delta} \psi_\delta(y, 0))^\dagger \rangle \\ &= - \frac{1}{L_x} \frac{1}{L_y} \sum_{x,y} \langle (\bar{\psi}_\alpha(x, t) (\gamma_5)_{\alpha\beta} \psi_\beta(x, t)) (\bar{\psi}_\delta(y, 0) (\gamma_5)_{\delta\gamma} \psi_\gamma(y, 0)) \rangle \\ &= - \frac{1}{L_x} \frac{1}{L_y} \sum_{x,y} \langle M^{-1}(x, t|x, t)_{\beta\alpha} M^{-1}(y, 0|y, 0)_{\gamma\delta} (\gamma_5)_{\alpha\beta} (\gamma_5)_{\delta\gamma} \rangle \\ & \quad + \frac{1}{L_x} \frac{1}{L_y} \sum_{x,y} \langle M^{-1}(y, 0|x, t)_{\gamma\alpha} M^{-1}(x, t|y, 0)_{\beta\delta} (\gamma_5)_{\alpha\beta} (\gamma_5)_{\delta\gamma} \rangle . \end{aligned} \quad (6.7)$$

This is the entry of one matrix element we have to compute. The example is for a rather simple interpolator. In the simulation also more complex ones are used, which, however, can be treated in a similar way.

For the correlators we also need to evaluate the conjugate interpolator. The general formula for this reads

$$\begin{aligned}
 O^\dagger(x, t) &= [ \bar{\psi}(x, t) \Gamma \psi(x, t) ]^\dagger \\
 &= [ \psi(x, t)^\dagger \gamma_2 \Gamma \psi(x, t) ]^\dagger \\
 &= \psi(x, t)^\dagger \Gamma \gamma_2 \psi(x, t) \\
 &= \pm (\bar{\psi}(x, t) \Gamma \psi(x, t)) ,
 \end{aligned} \tag{6.8}$$

with

$$\text{sign} = \begin{cases} + & \text{for } \Gamma = \gamma_2, \mathbb{1} \\ - & \text{for } \Gamma = \gamma_1, \gamma_5 . \end{cases} \tag{6.9}$$

## 6.2 Derivative sources

It is now possible to create an interpolator with fields  $\psi(x + n, t)$ ,  $\bar{\psi}(x + n, t)$ . This means, we go along the  $x$  direction a number of neighbours  $n$ , away from the central point  $x$  of the interpolator. If the number  $n$  is equal to zero the fermion fields  $\bar{\psi}$  and  $\psi$  are located at the same point and we are back at the simple interpolator (6.1).

In general, all interpolators which have the same quantum numbers describe the same state. However, some interpolators will be more relevant than others. The overlap between the interpolating fields and physical states can be improved by using more realistic spatial wave functions. Using the above introduced shifting, we construct more general interpolators, such as

$$O(x, t) = \sum_{x+n_1, x+n_2} f(x; x+n_1, x+n_2)_{\alpha_1, \alpha_2} \bar{\psi}(x+n_1, t)_{\alpha_1} \psi(x+n_2, t)_{\alpha_2} . \tag{6.10}$$

$f(x; x+n_1, x+n_2)$  is the spatial distribution function, which combines the fermionic fields  $\bar{\psi}(x+n_1, t)$  with  $\psi(x+n_2, t)$  at spatial positions  $x+n_1$ ,  $x+n_2$  in the vicinity of  $x$ . By setting  $f$  to

$$f(x; x+n_1, x+n_2)_{\alpha_1, \alpha_2} = \delta_{0, n_1} \delta_{\alpha_0 \alpha_1} \Gamma_{\alpha_0 \beta_0} \delta_{0, n_2} \delta_{\beta_0 \alpha_2} , \tag{6.11}$$

we get back the local interpolator

$$O(x, t) = \bar{\psi}(x, t)_{\alpha_0} \Gamma_{\alpha_0 \beta_0} \psi(x, t)_{\beta_0} . \tag{6.12}$$

A more realistic interpolator is obtained by not choosing a point-like source with all fields at a single spatial point. Instead we distribute them among several lattice sites, thus allowing at least a simple spatial wave function.

Furthermore it is possible to have a relative minus sign between the displaced fields which gives rise to a derivative source. Thus, combinations with a plus and with a minus sign inbetween are possible. If we are using a derivative source, a  $\gamma_1$  has also to be inserted because it means a derivation in the spatial  $\hat{1}$  direction. Hence, the correct construction for derivative sources is

$$\gamma_1 [\psi(x + n, t) - \psi(x - n, t)] . \quad (6.13)$$

Combining different choices for the Dirac matrix  $\Gamma$  with various shifted and derivative sources we come up with the following list of interpolators.

#### List of negative parity interpolators

$$\begin{aligned} O_1(t) &= \bar{\psi}(x + n, t) \gamma_5 \psi(x - n, t) \\ O_2(t) &= \bar{\psi}(x + n, t) \gamma_1 \psi(x - n, t) \\ O_3(t) &= \frac{1}{2} \bar{\psi}(x, t) \gamma_5 [\psi(x + n, t) + \psi(x - n, t)] \\ O_4(t) &= \frac{1}{2} \bar{\psi}(x, t) \gamma_1 [\psi(x + n, t) + \psi(x - n, t)] \\ O_5(t) &= \frac{1}{4} [\bar{\psi}(x + m, t) + \bar{\psi}(x - m, t)] \gamma_5 [\psi(x + n, t) + \psi(x - n, t)] \\ O_6(t) &= \frac{1}{4} [\bar{\psi}(x + m, t) + \bar{\psi}(x - m, t)] \gamma_1 [\psi(x + n, t) + \psi(x - n, t)] \\ O_8(t) &= \frac{1}{4} [\bar{\psi}(x + m, t) + \bar{\psi}(x - m, t)] [\psi(x + n, t) - \psi(x - n, t)] \\ O_9(t) &= \frac{1}{4} [\bar{\psi}(x + m, t) - \bar{\psi}(x - m, t)] \gamma_5 [\psi(x + n, t) - \psi(x - n, t)] \\ O_{10}(t) &= \frac{1}{4} [\bar{\psi}(x + m, t) - \bar{\psi}(x - m, t)] \gamma_1 [\psi(x + n, t) - \psi(x - n, t)] \end{aligned} \quad (6.14)$$

The positive parity interpolators turn out to not decay exponentially and instead correspond to a condensate. Thus we do not give a full list of interpolators.

## 6.3 Symmetries and quantum numbers

Let us now discuss the discrete symmetries parity  $\mathbf{P}$ , time reflection  $\mathbf{T}$  and charge conjugation  $\mathbf{C}$  of the interpolators used in our simulation. The quantum number  $\mathbf{J}$ , which stands for the angular momentum, does not exist in  $1 + 1$  dimensions, since there is just one spatial direction.

In order to check the quantum numbers of the interpolators one has to perform discrete symmetry transformations.

### 6.3.1 Parity

The parity transformation  $\mathbf{P}$  acts on our lattice fields as follows,

$$\psi(x, t) \xrightarrow{\mathbf{P}} \psi(x, t)^{\mathbf{P}} = \gamma_2 \psi(-x, t) , \quad (6.15)$$

$$\bar{\psi}(x, t) \xrightarrow{\mathbf{P}} \bar{\psi}(x, t)^{\mathbf{P}} = \bar{\psi}(-x, t) \gamma_2 . \quad (6.16)$$

It is obvious that the sign of the spatial coordinate  $x$  is flipped. In order to construct an eigenstate of  $\mathbf{P}$  we need to project to zero momentum. The general form of a Fourier transformation is

$$\hat{f}(p) = \frac{1}{L_x} \sum_x e^{-ipx} f(x) , \quad (6.17)$$

and for zero momentum it is

$$\hat{f}(p = 0) = \frac{1}{L_x} \sum_x f(x) . \quad (6.18)$$

For the check of the quantum numbers we use the following important relation:

$$\sigma_i \sigma_j + \sigma_j \sigma_i = 0 . \quad (6.19)$$

The  $\sigma_i$  are the Pauli matrices which are the 2-dimensional representation of the Dirac matrices  $\gamma_i$ , see App. B. The transformations for our operators are (our first example is a pseudoscalar and  $\Gamma = \gamma_5$ ):

- $O(t) = \sum_x \bar{\psi}(x, t) \gamma_5 \psi(x, t) \xrightarrow{\mathbf{P}} O(t)^{\mathbf{P}}$

$$\begin{aligned}
O(t)^{\mathbf{P}} &= \sum_x \bar{\psi}(-x, t) \gamma_2 \gamma_5 \gamma_2 \psi(-x, t) \\
&= - \sum_x \bar{\psi}(-x, t) \gamma_5 \psi(-x, t) \\
&= - \sum_y \bar{\psi}(y, t) \gamma_5 \psi(y, t) = -O(t) , \tag{6.20}
\end{aligned}$$

with the substitution  $-x = y$ . Thus we see that the pseudoscalar has negative parity as expected of course.

For an operator with displaced  $\psi$ 's we obtain in a similar way:

- $O(t) = \sum_x \bar{\psi}(x, t) \gamma_5 \frac{1}{2} [\psi(x+n, t) + \psi(x-n, t)]$

$$\begin{aligned}
O(t)^{\mathbf{P}} &= \sum_x \bar{\psi}(-x, t) \gamma_2 \gamma_5 \gamma_2 \frac{1}{2} [\psi(-x-n, t) + \psi(-x+n, t)] \\
&= - \sum_y \bar{\psi}(y, t) \gamma_5 \frac{1}{2} [\psi(y-n, t) + \psi(y+n, t)] \\
&= - \sum_y \bar{\psi}(y, t) \gamma_5 \frac{1}{2} [\psi(y+n, t) + \psi(y-n, t)] = -O(t) . \tag{6.21}
\end{aligned}$$

Additionally for an operator with a derivative source we find:

- $O(t) = \sum_x \bar{\psi}(x, t) \gamma_5 \gamma_1 \frac{1}{2} [\psi(x+n, t) - \psi(x-n, t)]$

$$\begin{aligned}
O(t)^{\mathbf{P}} &= \sum_x \bar{\psi}(-x, t) \gamma_2 \gamma_5 \gamma_1 \gamma_2 \frac{1}{2} [\psi(-x-n, t) - \psi(-x+n, t)] \\
&= \sum_y \bar{\psi}(y, t) \gamma_5 \gamma_1 \frac{1}{2} [\psi(y-n, t) - \psi(y+n, t)] \\
&= - \sum_y \bar{\psi}(y, t) \gamma_5 \gamma_1 \frac{1}{2} [\psi(y+n, t) - \psi(y-n, t)] = -O(t) . \tag{6.22}
\end{aligned}$$

Thus, all types of operators we use in the pseudoscalar channel have negative parity as expected. For the scalar interpolators the determination of the parity (they have positive parity) works the same way. A full list of the quantum numbers is found in Table 6.1.

state	$PC$	$\Gamma$
positive parity	$++$	$\mathbb{1}, \gamma_2$
negative parity	$--$	$\gamma_5, \gamma_1$

**Table 6.1:** Overview of the quantum numbers of our interpolators. Positive parity states always have  $\mathbf{C} = +1$ , while negative parity states have  $\mathbf{C} = -1$ . The  $\Gamma$  we have is augmented with an additional  $\gamma_1$  for each derivative source (compare the list of interpolators (6.14)).

### 6.3.2 Time reflection

In Euclidean space parity and time reflection are completely equivalent. For completeness, the time reflection acts on our spinors as

$$\psi(x, t) \xrightarrow{\mathbf{T}} \psi(x, t)^{\mathbf{T}} = \gamma_1 \psi(x, -t) , \quad (6.23)$$

$$\bar{\psi}(x, t) \xrightarrow{\mathbf{T}} \bar{\psi}(x, t)^{\mathbf{T}} = \bar{\psi}(x, -t) \gamma_1 . \quad (6.24)$$

### 6.3.3 Charge conjugation

The charge conjugation  $\mathbf{C}$  (see Appendix B) acts on our spinor fields and transforms particles and anti-particles in the following way,

$$\begin{aligned} \psi(x, t) &\xrightarrow{\mathbf{C}} \psi(x, t)^{\mathbf{C}} = C^{-1} \bar{\psi}(x, t)^T , \\ \bar{\psi}(x, t) &\xrightarrow{\mathbf{C}} \bar{\psi}(x, t)^{\mathbf{C}} = -\psi(x, t)^T C . \end{aligned} \quad (6.25)$$

$C$  is the charge conjugation matrix, which acts only on the Dirac indices. The matrix  $C$  obeys the relation

$$C \gamma_\mu C^{-1} = -\gamma_\mu^T . \quad (6.26)$$

In our representation  $C$  is given by  $C = i\gamma_2$ . We will now show the result of a charge conjugation on an interpolator which stays invariant (projection to zero momentum is omitted here for notational convenience):

- $O(t) = \sum_x \bar{\psi}(x, t) \mathbb{1} \psi(x, t) \xrightarrow{\mathbf{C}} O(t)^{\mathbf{C}}$

$$\begin{aligned}
O(t)^{\mathbf{C}} &= - \sum_x \psi(x, t)^T C C^{-1} \bar{\psi}(x, t)^T \\
&= - \sum_x \psi(x, t)^T \bar{\psi}(x, t)^T = \sum_x \bar{\psi}(x, t) \psi(x, t) = O(t) . \quad (6.27)
\end{aligned}$$

An example for a charge conjugation of a pseudoscalar interpolator is:

$$\begin{aligned}
\bullet \quad O(t) &= \sum_x \bar{\psi}(x, t) \gamma_5 \psi(x, t) \xrightarrow{\mathbf{C}} O(t)^{\mathbf{C}} \\
O(t)^{\mathbf{C}} &= - \sum_x \psi(x, t)^T C \gamma_5 C^{-1} \bar{\psi}(x, t)^T \\
&= \sum_x \psi(x, t)^T C \gamma_5^T C^{-1} \bar{\psi}(x, t)^T \\
&= - \sum_x \bar{\psi}(x, t) \gamma_5 \psi(x, t) = -O(t) . \quad (6.28)
\end{aligned}$$

Here we used the relation (6.26). As one can see, under charge conjugation this interpolator gets a minus sign. Our last example is a negative parity interpolator with a displaced source:

$$\begin{aligned}
\bullet \quad O(t) &= \frac{1}{2} \sum_x \bar{\psi}(x, t) \gamma_5 [\psi(x+n, t) + \psi(x-n, t)] \\
O(t)^{\mathbf{C}} &= -\frac{1}{2} \sum_x \psi(x, t)^T C \gamma_5 C^{-1} [\bar{\psi}(x+n, t)^T + \bar{\psi}(x-n, t)^T] \\
&= \frac{1}{2} \sum_x \psi(x, t)^T \gamma_5^T [\bar{\psi}(x+n, t)^T + \bar{\psi}(x-n, t)^T] \\
&= -\frac{1}{2} \sum_x [\bar{\psi}(x+n, t) \gamma_5 \psi(x, t) + \bar{\psi}(x-n, t) \gamma_5 \psi(x, t)] \\
&= -\frac{1}{2} \sum_y \bar{\psi}(y, t) \gamma_5 [\psi(y+n, t) + \psi(y-n, t)] \\
&= -O(t) . \quad (6.29)
\end{aligned}$$

In the first term we substituted  $y = x + n$  and in the second  $y = x - n$ . From the result we see that the interpolator  $O(t)$  transforms into  $-O(t)$ .

The symmetry transformations will not be presented for all interpolators we use, but a list of the quantum numbers is given in Table 6.1. The positive parity interpolators always have  $\mathbf{C} = +1$ , while the negative parity is tied to  $\mathbf{C} = -1$ .

We finally mention that the action (2.10) is invariant under all the three transformations. The time reflection plays an important role for the reconstruction of

the Hilbert space for the Minkowski theory. For that it is also important to impose anti-periodic temporal boundary conditions for the fermions. That is why we set the boundary conditions anti-periodic in time in our numerical calculations.



# Chapter 7

## Excited state spectroscopy

So far we have prepared the ground for computing excited states. We know the model, how to produce different configurations of the scalar field  $\Phi$ , and how to compute the raw data out of the correlation matrix  $C(t)_{ij}$ . Now we discuss how to extract the masses of the excited states from the correlation matrix.

Spectroscopy of excited states is not a trivial task. In Hilbert space a correlator is an infinite sum of exponentials.

$$C(t) = a_0 e^{-tE_0} + a_1 e^{-tE_1} + \dots, \quad (7.1)$$

with  $E_0 < E_1 < E_2 \dots$  being the energy levels of the states. The leading exponential involves the ground state energy  $E_0$ , while the excited levels  $E_1, E_2, \dots$  appear only as subleading terms.

### 7.1 The variational method

The tool we are going to use is the variational method [2, 3]. The key idea is, as outlined in the previous chapter, to work with several linearly independent interpolators  $O_i, i = 1, \dots, r$ . These interpolators all have the same quantum numbers corresponding to the state we want to construct. The correlation matrix has the following form:

$$C(t)_{ij} = \langle O_i(t) O_j^\dagger(0) \rangle \quad i, j = 1, 2, \dots, r. \quad (7.2)$$

The correlator has the spectral decomposition

$$C(t)_{ij} = \sum_{n=1}^{\infty} a_i^{(n)} a_j^{(n)*} e^{-tE_n} , \quad (7.3)$$

with

$$a_i^{(n)} = \langle 0|O_i|n\rangle . \quad (7.4)$$

$E_n$  denotes the energy of the state  $|n\rangle$ . In the analysis we first truncate the spectral sum of the matrix after the  $r$ -th term, treating the omitted terms as a perturbation. The truncated hermitian  $r \times r$  matrix  $\tilde{C}(t)$  then is defined as

$$\tilde{C}(t)_{ij} = \sum_{n=1}^r a_i^{(n)} a_j^{(n)*} e^{-tE_n} . \quad (7.5)$$

We assume that the coefficients  $a_i^{(n)}$  form a matrix of full rank. We consider now the generalised eigenvalue problem

$$\tilde{C}(t) \vec{v}^{(k)} = \lambda(t)^{(k)} \tilde{C}(t_0) \vec{v}^{(k)} . \quad (7.6)$$

Following [30] we insert (7.5) in (7.6) and find

$$\sum_{n=1}^r a_i^{(n)} \rho^{(n,k)} [e^{-tE_n} - \lambda(t)^{(k)} e^{-t_0E_n}] = 0 , \quad (7.7)$$

with the coefficients

$$\rho^{(n,k)} = \sum_{j=1}^r a_j^{(n)*} v_j^{(k)} . \quad (7.8)$$

Since the coefficients  $a_i^{(n)}$  have full rank, which means the determinant  $\det(a_i^{(n)})$  does not vanish, the  $a_i^{(n)}$  are linearly independent. Furthermore this implies, that a linear combination  $\sum_n \alpha_n \vec{a}^{(n)} = 0$  is not possible to realise non trivially, and that this relation just holds for  $\alpha_n = 0$ . From this argument it follows that in our case the  $\alpha_n$  are represented by

$$\rho^{(n,k)} [e^{-tE_n} - \lambda(t)^{(k)} e^{-t_0E_n}] = 0 \quad \forall n . \quad (7.9)$$

Let us assume that  $\rho^{(n,k)} = 0 \forall k$ . This means that

$$\sum_{j=1}^r a_j^{(n)*} v_j^{(k)} = 0 \quad \forall k . \quad (7.10)$$

The  $v_j^{(k)}$  also form a matrix of full rank. As a consequence the  $a_j^{(n)*}$  have to be zero, which is a contradiction to the full rank of  $a_j^{(n)*}$ . This leads to the only possible conclusion that  $\rho^{(n,k)} \neq 0$ . So the term in the parentheses of (7.7) has to be zero and hence the eigenvalues are given by

$$\lambda(t)^{(k)} = e^{-E^{(k)}(t-t_0)} . \quad (7.11)$$

By returning to the full matrix  $C(t)$ , we have to add terms of  $\mathcal{O}(\exp(-tE_{r+1}))$ . As a matter of fact, in second order of perturbation theory also terms of  $\mathcal{O}(\exp(-tE_k))$ ,  $k \leq r$  reappear.

The complete eigenvalues of  $C(t)$  are then

$$\lambda(t)^{(k)} = e^{-E^{(k)}(t-t_0)} [1 + \mathcal{O}(e^{-(t-t_0)\Delta_k})] , \quad (7.12)$$

where  $E_k$  is the energy of the  $k$ -th state and  $\Delta_k$  is the energy difference to neighbouring states.

As one can see, with the variational technique we have found a way to calculate the groundstate as well as excited states, given by the corresponding eigenvalues. In the next section we will discuss how to extract the mass out of the exponential.

## 7.2 Effective masses

The ground state energy can be computed by directly analysing the correlation function without using the variational technique. In principle, it makes sense to first just look on the lowest energy level of (7.5) - the ground state  $E_0$ , to get an impression of the behaviour of the used interpolators. If one takes into account propagation forward in time  $t$  and backward  $(L_t - t)$ , the correlator will show a cosh-behaviour. For the ground state it leads to

$$C(t) = a_0 e^{-tE_0} + a_0 e^{-(L_t-t)E_0} = 2 a_0 e^{-L_t \frac{E_0}{2}} \cosh\left(\left(\frac{L_t}{2} - t\right)E_0\right) . \quad (7.13)$$

$C(t)$  can either be a simple correlator or any entry of the correlation matrix.

Naively one can define an *effective mass* as

$$m_{\text{eff}}\left(t + \frac{1}{2}\right) = \ln \frac{C(t)}{C(t+1)} . \quad (7.14)$$

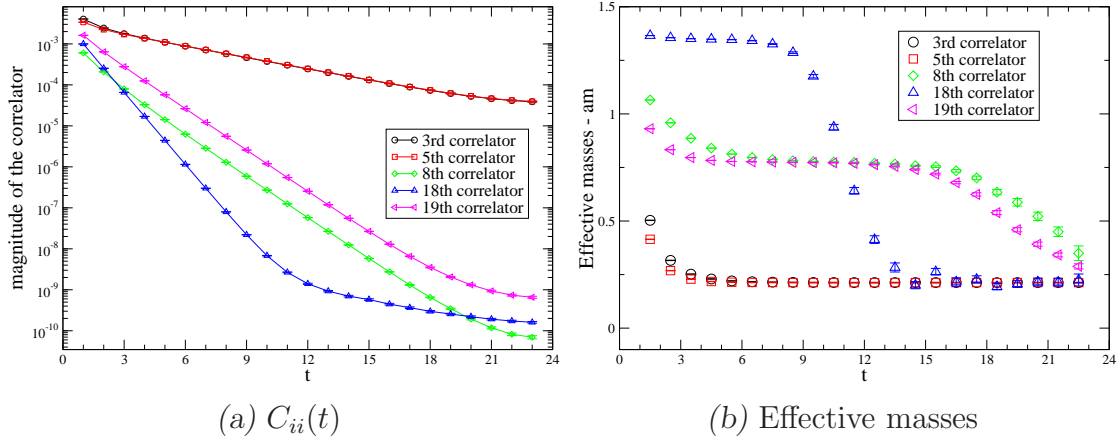


**Figure 7.1:** We show the diagonal entries  $C_{ii}(t)$  of the correlation matrix (a) and the corresponding effective masses (b) for a  $16 \times 48$  lattice, with  $g = 0.05$ ,  $m = 0.05$  and  $N_f = 2$ . The correlation matrix has been built out of 5 interpolators, which can be looked up in the list of Eq. (6.14). In our simulation we used a set with  $m = n = 3$  ( $O_1, \dots, O_{10}$ ) and a set with  $m = 4, n = 2$  ( $O_{11}, \dots, O_{20}$ ). All diagonal entries of the correlation matrix have a cosh-behaviour. This look at the correlation matrix gives us an idea which interpolators couple to higher excitations.

If one respects periodicity in time according to Eq. (7.13), one can also consider

$$\frac{C(t)}{C(t+1)} = \frac{\cosh(m_{\text{eff}}(t - \frac{L_t}{2}))}{\cosh(m_{\text{eff}}(t+1 - \frac{L_t}{2}))}, \quad (7.15)$$

and compute  $m_{\text{eff}}$  numerically from this relation, as has been done in Fig. 7.1. This means one has to search for which value of  $m_{\text{eff}}$  the following equation holds

$$C(t) \cosh(m_{\text{eff}}(t+1 - L_t/2)) - C(t+1) \cosh(m_{\text{eff}}(t - L_t/2)) = 0. \quad (7.16)$$

The same strategy for defining effective masses can be applied to the eigenvalues of the correlation matrix, and, e.g., for the simple definition we obtain

$$m_{\text{eff},k}(t, t_0) = \ln \frac{\lambda_k(t, t_0)}{\lambda_k(t+1, t_0)}. \quad (7.17)$$

The computation of the effective mass out of this formula, is reflected in Fig. 7.2.

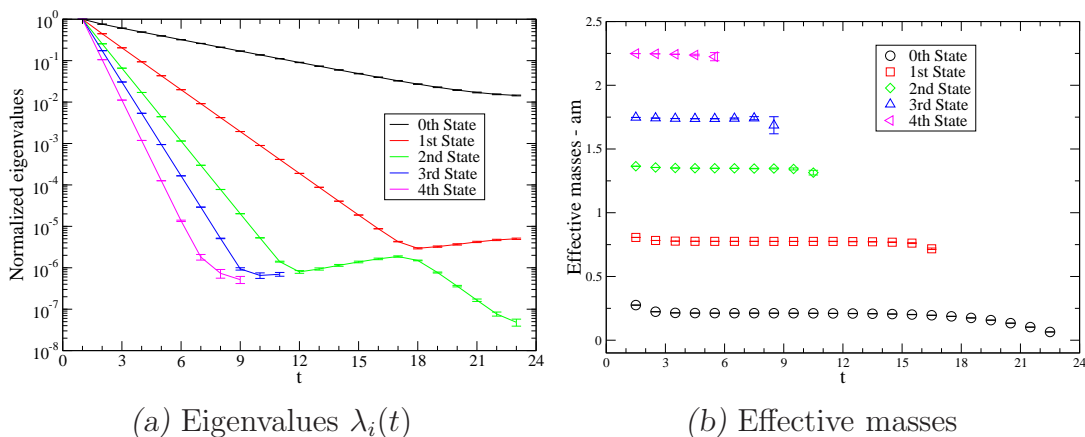


**Figure 7.2:** These two plots show the same as in Fig. 7.1, just with the difference, that the effective mass plateaus (b) have been computed from the eigenvalues of plot (a). By using the variational technique we get here 5 well separated plateaus.

Now we have everything we need, the only missing thing is a fit, to get the mass value of the ground state and the  $k$  excited states out of the plot. The effective masses discussed above are an important tool to determine the range of  $t$ -values for the fit.

### 7.3 Fit of the correlator

Consider a fit for the ground state mass. The excited masses will work in the same way. For our two-parameter fit we have to determine the parameters  $A$  and  $m$  in the fit function  $f_{A,m}(t)$  such that the  $\chi^2$ -functional is minimised,

$$\chi^2 = \sum_{t=t_{min}}^{t_{max}} (C(t) - f_{A,m}(t))^2. \quad (7.18)$$

$C(t)$  can either be a simple correlator or one of the eigenvalues of the correlation matrix. The summation runs over the minimum and maximum fit ranges, which can be read off directly from the effective mass plateaus. Our proposal for the fit-function will be

$$f_{A,m}(t) = A \cosh((L_t/2 - t) m) \quad \text{or} \quad f_{A,m}(t) = A \exp(-t m). \quad (7.19)$$

Here we discuss the calculation for the cosh-ansatz. The extremum condition implies

$$\frac{\partial \chi^2}{\partial A} = 0 \quad \text{and} \quad \frac{\partial \chi^2}{\partial m} = 0 . \quad (7.20)$$

The amplitude  $A$  can be computed in closed form as

$$A = \frac{\sum_t C(t) \cosh((L_t/2 - t) m)}{\sum_t \cosh^2((L_t/2 - t) m)} . \quad (7.21)$$

The second step is to insert  $A$  into Eq. (7.18). This leads to the following expression

$$\chi^2 = \sum_{t=t_{min}}^{t_{max}} \left( C(t) - \frac{\sum_{t'} C(t') \cosh((L_t/2 - t') m)}{\sum_{t'} \cosh^2((L_t/2 - t') m)} \cosh((L_t/2 - t) m) \right)^2 . \quad (7.22)$$

This gives rise to a transcendental equation which must be solved numerically to obtain  $m$ . The method can be applied to either a correlator or one of the eigenvalues, giving rise to either only the ground state mass or the ground- and excited states corresponding to the eigenvalues used.

# Chapter 8

## Evaluation of the data - results

This chapter presents the results which have been obtained out of the numerically produced raw data. The techniques for preparing the raw data have been explained in the last chapters. Especially Chapters 6 and 7 provide us on the one hand with the used interpolators and their symmetries, and on the other hand with the variational method for gaining the effective masses.

As a reminder we again list the interpolators used:

$$\begin{aligned} O_1(t) &= \bar{\psi}(x+n, t) \gamma_5 \psi(x-n, t) \\ O_2(t) &= \bar{\psi}(x+n, t) \gamma_1 \psi(x-n, t) \\ O_3(t) &= \frac{1}{2} \bar{\psi}(x, t) \gamma_5 [\psi(x+n, t) + \psi(x-n, t)] \\ O_4(t) &= \frac{1}{2} \bar{\psi}(x, t) \gamma_1 [\psi(x+n, t) + \psi(x-n, t)] \\ O_5(t) &= \frac{1}{4} [\bar{\psi}(x+m, t) + \bar{\psi}(x-m, t)] \gamma_5 [\psi(x+n, t) + \psi(x-n, t)] \\ O_6(t) &= \frac{1}{4} [\bar{\psi}(x+m, t) + \bar{\psi}(x-m, t)] \gamma_1 [\psi(x+n, t) + \psi(x-n, t)] \\ O_8(t) &= \frac{1}{4} [\bar{\psi}(x+m, t) + \bar{\psi}(x-m, t)] [\psi(x+n, t) - \psi(x-n, t)] \\ O_9(t) &= \frac{1}{4} [\bar{\psi}(x+m, t) - \bar{\psi}(x-m, t)] \gamma_5 [\psi(x+n, t) - \psi(x-n, t)] \\ O_{10}(t) &= \frac{1}{4} [\bar{\psi}(x+m, t) - \bar{\psi}(x-m, t)] \gamma_1 [\psi(x+n, t) - \psi(x-n, t)] \end{aligned} \tag{8.1}$$

As can be seen, there exists no operator  $O_7$ . This is because we removed an interpolator from our original list due to wrong quantum numbers, but kept the numbers assigned to the other interpolators.  $m$  and  $n$  denote the relative shifts

in spatial direction. In our simulation we used a set with  $m = n = 3$  ( $O_1, \dots O_{10}$ ) and a set with  $m = 4, n = 2$  ( $O_{11}, \dots O_{20}$ ). All interpolators are projected to vanishing total momentum by summing over  $x$ . This specifies a complete set of 18 interpolators we are studying, and we refer to this numbering in the following plots. Our statistics is typically 400 configurations for each set of parameters (lattice size  $L$ , coupling constant  $g$  and bare mass  $m$ ). We here always discuss the plots only for  $N_f = 2$  flavors, since the dependence of the number of flavors will be addressed separately in Sec. 8.8.

## 8.1 Diagonal correlators

An important tool for analysing the behaviour of all interpolators is to directly look at the diagonal entries of the correlation matrix. It can give us a hint which interpolator will probably couple to higher excited states. For that analysis it is also very interesting to look at a rather long time evolution  $t$ .

As one can see in Fig. 8.1(a), the interpolators with a relative minus sign (derivative interpolators) show a steeper slope compared to the interpolators with a relative plus sign, indicating that they strongly couple to excitations. We stress, however, that also the derivative interpolators couple to the ground state as can be seen in the effective mass plots 8.1(b). They show a second plateau at the ground state mass for large values of  $t$ . Interpolator  $O_{18}$  even seems to couple to a higher excited state, but settles at the ground state beyond  $t \approx 13$ .

These two plots indicate that if we want to find higher excited states, we always should include derivative sources in our correlation matrix. Especially  $O_{18}$  should be included, since it couples to an even higher state.

## 8.2 Effective mass plateaus

We now present a few effective mass plateaus to get an idea of the dependence of the fit mass on the bare mass. In our calculations we use the 4 values  $m = 0.01, 0.05, 0.1, 0.2$  for the bare mass for each value of  $g$ .

In Fig. 8.2 and Fig. 8.3 we compare the plateaus for the two coupling constants  $g = 0.01$  and  $g = 0.1$ . Apparently, in both plots the excited states are quite insensitive to a change of the bare mass  $m$ . Only the ground state varies somewhat

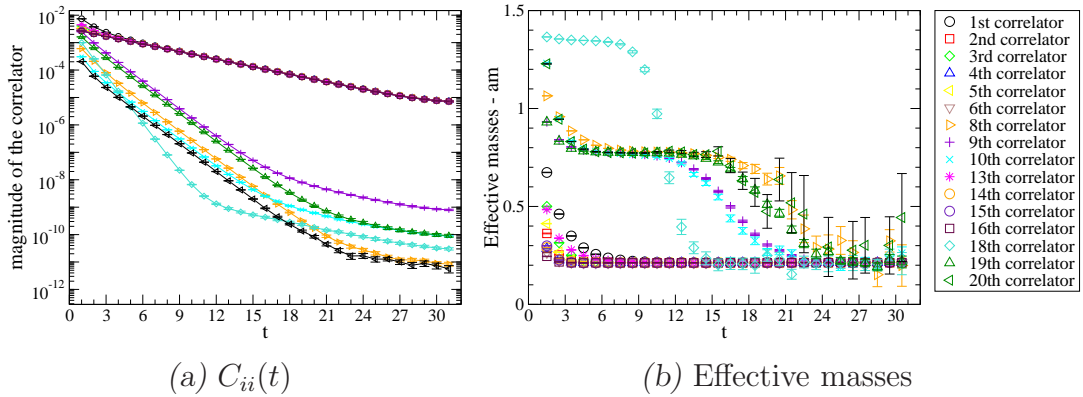


**Figure 8.1:** We show the diagonal entries  $C_{ii}(t)$  of the correlation matrix and the corresponding effective masses for a  $16 \times 64$  lattice, with  $g = 0.05$ ,  $m = 0.05$  and  $N_f = 2$ .

stronger. The effect of the increasing coupling constant  $g$  comes not out quite clearly here. In Section 8.4 the connection should be seen better in a different kind of plot.

For the final analysis the effective masses are computed from Eq. (7.17), i.e., out of the eigenvalues of the correlation matrix  $C(t)$ . Thus, it makes sense to look also directly at the eigenvalues  $\lambda(t)$ , which are plotted in Fig. 8.4 and 8.5. They mirror what we can already see in the effective mass plots of Fig. 8.2 and 8.3. The steeper slope corresponds to the higher excited states, which consequently have shorter plateaus.

It is interesting to observe in Fig. 8.4 and Fig. 8.5, that the propagators running forward in time, mix with the contributions of the propagators running backward in time. It comes to the formation of shoulders within the eigenvalues. From that we can see that the separation of the different physical states into distinct eigenvalues of the generalised eigenvalue problem works only for forward propagation.

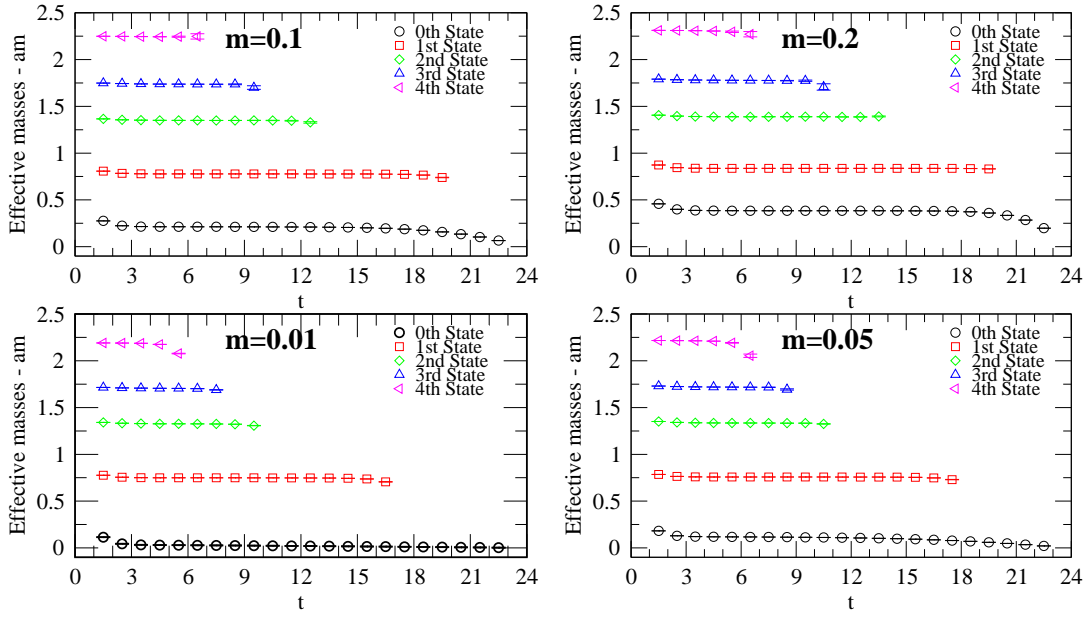


Figure 8.2: Effective mass plots for the eigenvalues of the correlation matrix. Lattice size  $L = 16 \times 48$ ,  $g = 0.01$ ,  $m = 0.01, 0.05, 0.1, 0.2$ .

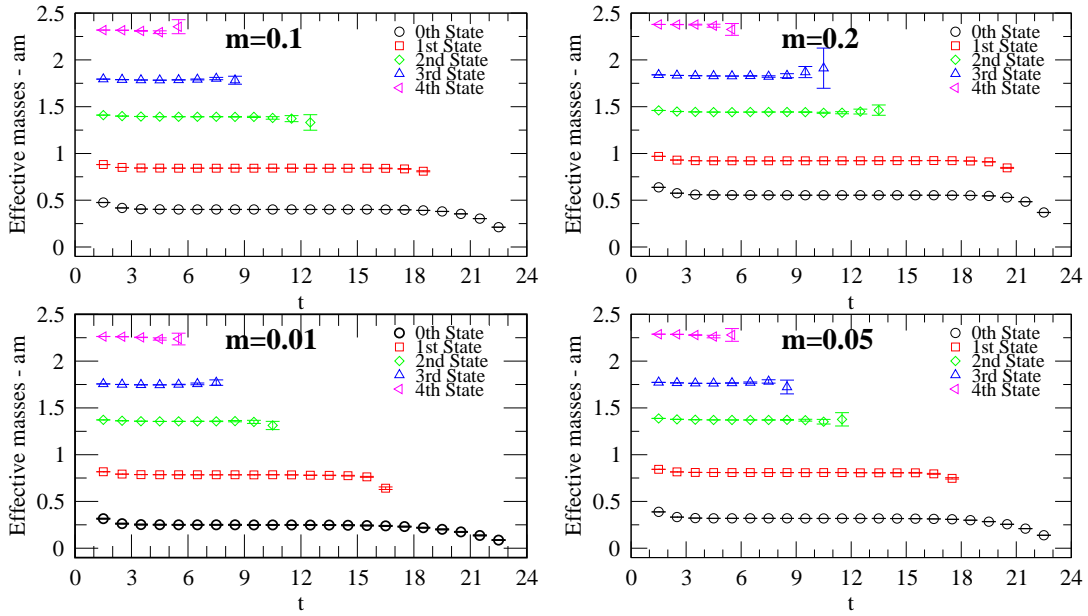
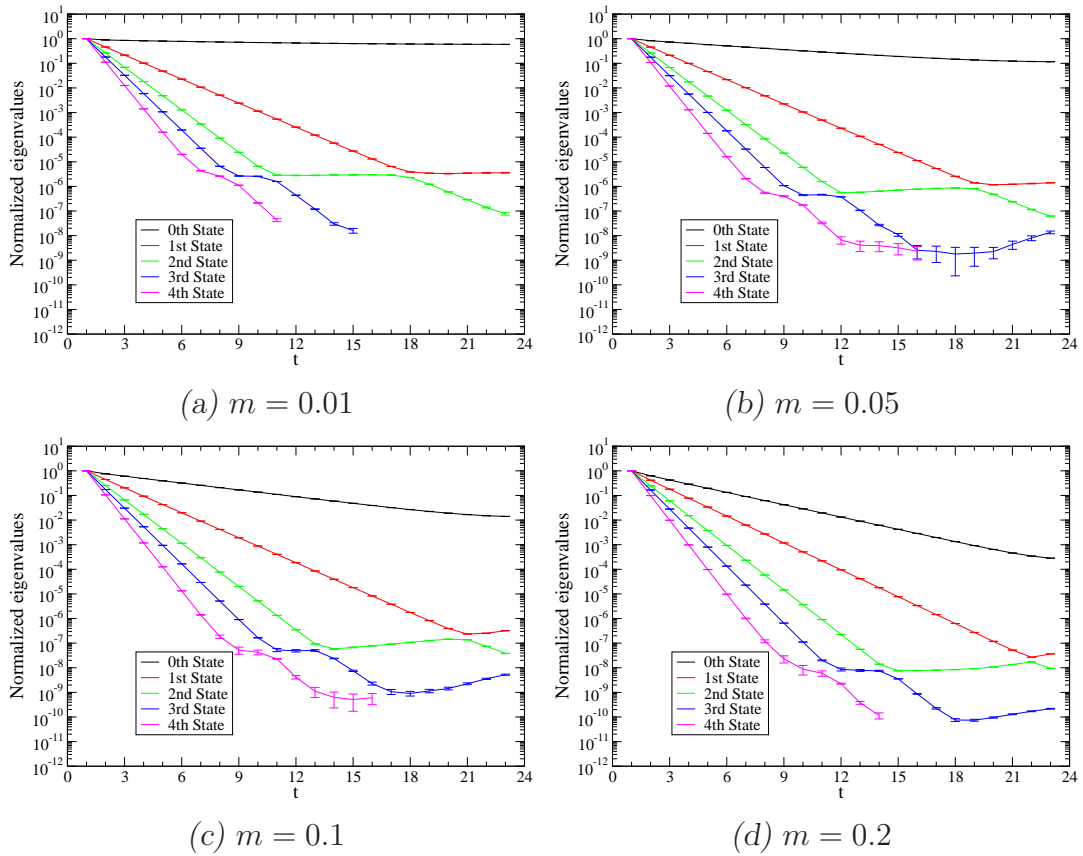


Figure 8.3: Same as Fig. 8.2, now for  $g = 0.1$ .



**Figure 8.4:** Plot of the eigenvalues corresponding to the effective masses of Fig. 8.2. Lattice size  $L = 16 \times 48$ ,  $g = 0.01$ .

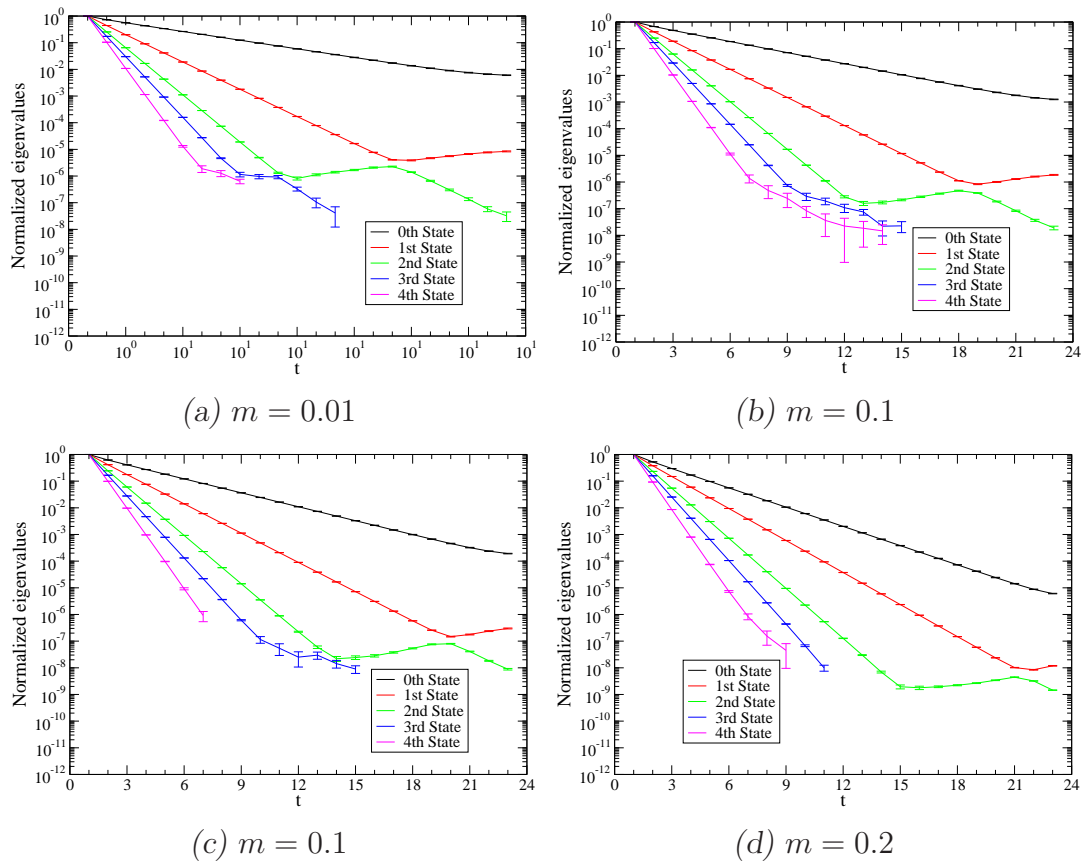
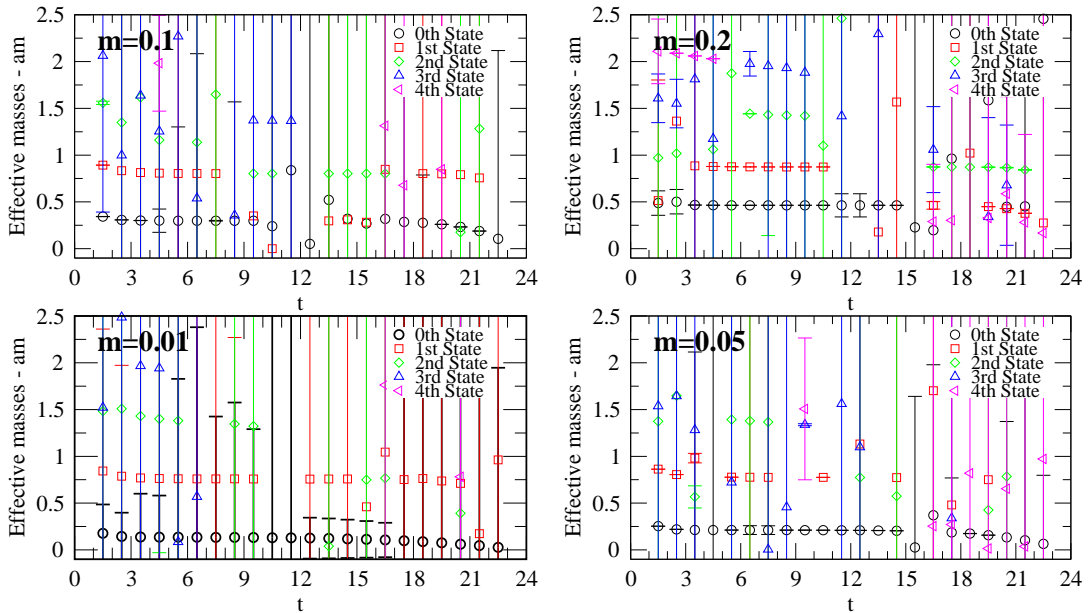


Figure 8.5: Same as Fig. 8.4, now for  $g = 0.1$ .



**Figure 8.6:** Example of effective mass plateaus for a bad choice of interpolators. Lattice size  $L = 16 \times 48$ ,  $g = 0.05$ .

### 8.3 Choice of interpolators

In our calculations we produce the raw data for 18 interpolators. When we correlate them, we only use a subset of those 18. The difficulty is now, to find out which ones we should use in the final correlation matrix. In Sec. 8.1 we already mentioned that a hint is given by looking at the diagonal of the correlation matrix for all 18 interpolators. There one can check which interpolator couples to higher excited states, and which one will probably not. This can be seen in Fig. 8.1(a), where obviously only the interpolators with a derivative source couple to higher excitations.

However, the leading criterion for the choice of interpolators in the correlation matrix, is the quality of the effective mass plateaus, calculated out of the eigenvalues. If we find long plateaus, with a good quality, we know that our choice has been a good one. For illustration purposes, we give an example of a poor combination of interpolators in Fig. 8.6. Here we have combined 3, 5, 9, 13, 19,

while the optimal choice consists of interpolators 3, 5, 8, 18, 19. These plateaus are shaky with large error bars and can not be used in fits for the ground state mass and the higher excited states masses. Additionally, although they are a combination of five interpolators, they just form four plateaus, and those are not very good.

Let us assume that we have found a good combination of interpolators, showing 4 proper plateaus. An interesting fact is, that the plateaus are essentially invariant under a change of the choice of the interpolators. It is always possible to find another combination of interpolators which form plateaus at the same position. The difference can just be seen in the fact, that sometimes, some interpolators have smaller error bars, and that are the ones we should of course use in the final analysis.

In the whole, it is still not an easy task to find the best combinations. It is a trial and error business with a little bit of gut feeling. And there is still the open question, how many excited states, one really will get out of the correlation matrix. Here, we always produced a ground state and 4 higher excited states. But maybe, with another combination or more interpolators, one might be able to extract even more states.

## 8.4 Mass dependence of the spectrum

After we have performed the fits of the different eigenvalues from now on we denote the energy values as  $M_i$ , using  $M_0$  for the ground state,  $M_1$  for the first excitation, etc.

An important question is how the spectrum depends on the mass parameter  $m$ . In Fig. 8.7 we plot the masses of ground- and excited states as a function of  $m$ . The individual plots display our results for various values of the coupling  $g$ . In the figures we can observe that for a fixed coupling  $g$ , the spectrum is essentially a linear function of  $m$ . The slope differs slightly for the different states.

We can furthermore conclude from Fig. 8.7, that with increasing  $g$ , the energy values also increase. This can be seen by just comparing the mass value  $M_0 = 0.0251(04)$  at the bare mass  $m = 0.01$  with the coupling  $g = 0.01$ , while  $M_0 = 0.2497(12)$  for  $g = 0.1$ . Obviously the ground state mass increases with  $g$ . Or, if one looks, e.g., at the highest excited state with the bare mass  $m = 0.2$ , for

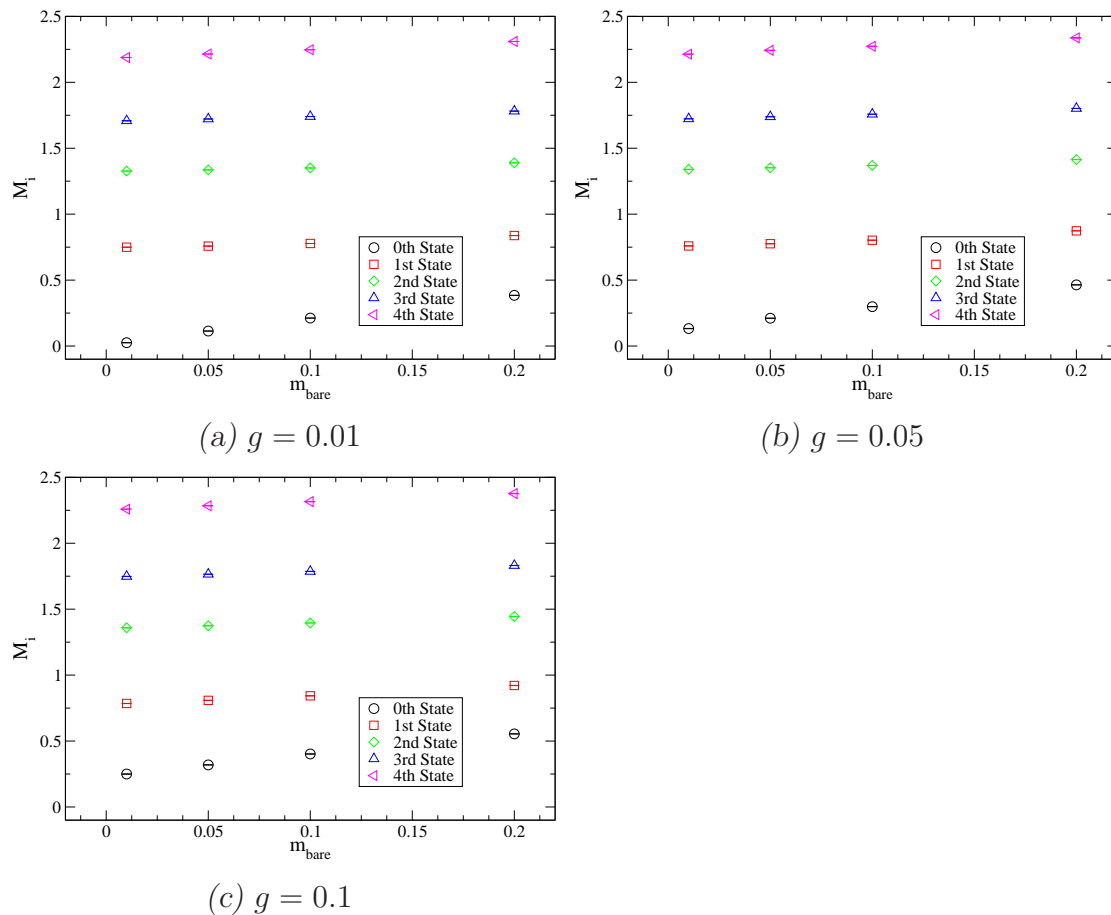


**Figure 8.7:** Plot of the mass spectrum  $M_i$  versus the bare mass  $m$  compared for 3 different values of the coupling constant  $g$ , for a  $16 \times 48$  lattice.

$g = 0.01$  one finds  $M_4 = 2.3097(02)$ , while at  $g = 0.1$  we have  $M_4 = 2.3771(15)$ .

## 8.5 Finite size effects - scattering states

If we want to find out about finite size effects, we have to produce data, for different lattice sizes. We generated configurations for lattice sizes of  $10 \times 48$ ,  $14 \times 48$ ,  $16 \times 48$ ,  $18 \times 48$ ,  $20 \times 48$  and  $22 \times 48$ .

Furthermore we varied the time extent and considered also a  $16 \times 64$  lattice. This lattice was for confirming that the operators which couple predominantly to excited states still develop an effective mass plateau at the position of the ground

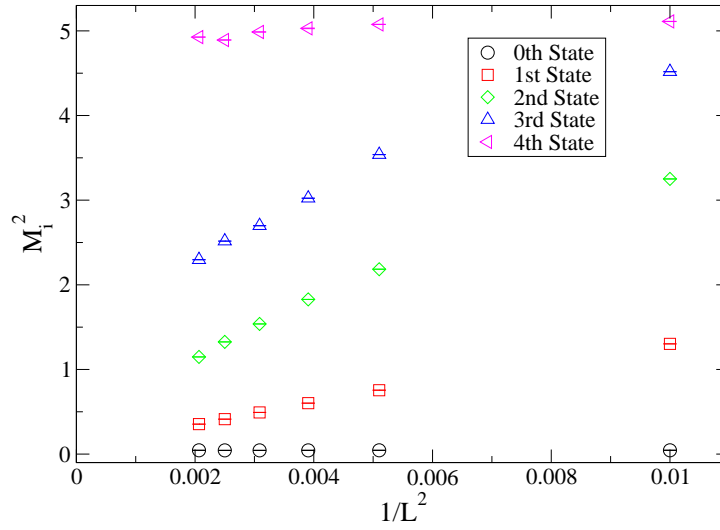


**Figure 8.8:** Squares of mass versus inverse volume squared. Lattice size  $L = 16 \times 48$ ,  $g = 0.05$  and  $m = 0.05$ .

state for sufficiently large  $t$ . This is indeed the case, as has been illustrated in Fig. 8.1.

But now we are coming back again to the volume effects. Plotting the spectrum versus  $1/L^2$ , where  $L$  is the spatial extent of the lattice, shows some interesting new results. Looking at Fig. 8.8, we see, that apparently, only the first three excitations show a volume dependence. The ground state and the fourth excited state, seem to be almost invariant under changes of the volume. Normally, the bound states should show no volume dependence (up to exponentially small corrections), as the ground state and the fourth excited state do. But scattering states, are volume dependent: In a finite box the relative momentum of two scattering particles has to be a multiple of the Matsubara frequency  $2\pi/L$ . This implies that scattering states should show a volume dependence as we observe for the first three excitations.

Following [3, 31, 32, 33] this volume dependence can be put on a quantitative level. To correctly interpret and understand our energy spectrum, we have to know something about the energy values of scattering states and their volume dependence.

In a finite volume the particle momenta are quantised and therefore the energy

spectrum of two particle states is discrete. The scattering phase shift  $\delta(k)$ , at a momentum  $k$ , in a finite volume, is given in one dimension by

$$\exp(2\pi in) \exp(2i\delta(k)) = \exp(-ikL) , \quad \text{with} \quad n = 0, 1, 2, \dots . \quad (8.2)$$

$L$  denotes the box size, thus the finite volume and the momentum  $k$  are related to the energy  $W$  through

$$W = 2\sqrt{m^2 + k^2} , \quad (8.3)$$

where  $m$  is the mass of the scattered particles. Using Eq. (8.2) we can express the momentum  $k$  as

$$k = \frac{2\pi n}{L} - \frac{2\delta(k)}{L} , \quad (8.4)$$

so that the energy becomes

$$W = 2\sqrt{m^2 + \frac{4}{L^2}(\pi n - \delta(k))^2} . \quad (8.5)$$

This is the energy of the scattering state in a finite volume. Thus in Fig. 8.8 and the figures below, we plot

$$W^2 \text{ versus } \frac{1}{L^2} , \quad (8.6)$$

and expect a linear behaviour.

In Fig. 8.9 we illustrate what happens with the wave function of our scattering states when we put them into a finite box. The top curve corresponds to the plane wave solution of the free case. The bottom curve shows the wave function where an attractive potential is located near the origin. There the frequency is larger, resulting in a phase shift at  $L/2$ .

As mentioned before, it seems that the ground state and the highest excited state are no scattering states, since there is no volume dependence. But it looks

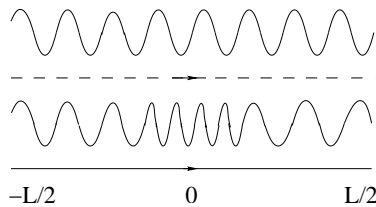


**Figure 8.9:** Solution of the Schrödinger equation for the non-interacting case  $V = 0$  (top plot), and for a short range attractive potential (bottom plot).

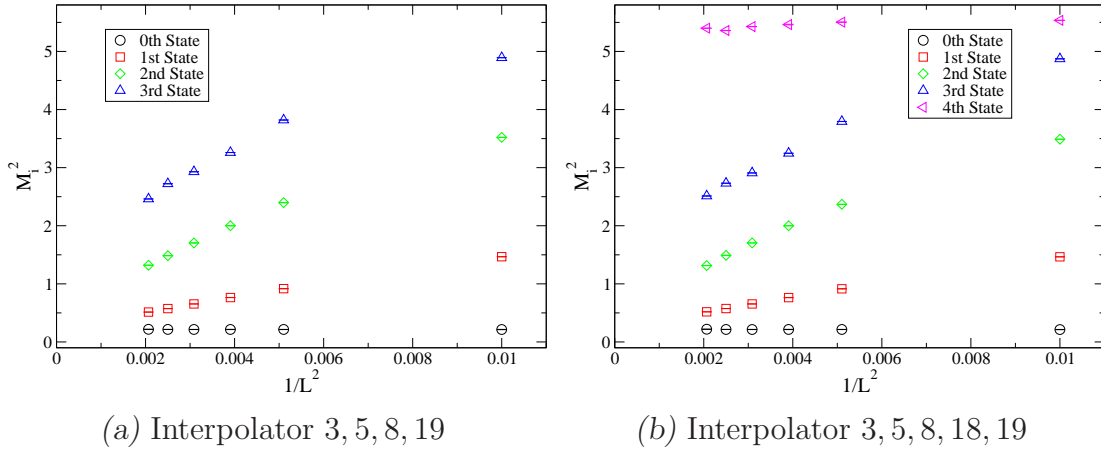


**Figure 8.10:** Comparison of the size dependence of 4 states and 5 states, for  $g = 0.05$  and  $m = 0.05$ .

as if the highest state is at least a little bit influenced by the volume. This is why we need to study the highest state in more detail, and see what happens with it, when we correlate instead of five interpolators, only four. Fig. 8.10 shows, that the fifth state just vanishes, and as one can see in Fig. 8.10(a), the highest state does not stabilise to a volume independent state. It rather stays a scattering state.

Thus we cannot exclude that  $M_4$  is an artifact of the variational method caused by the limited choice of our basis.

## 8.6 The eigenvectors of the eigenvalue problem

Until now, we have not used the eigenvectors of the generalised eigenvalue problem. Fact is, they are very interesting for us, because they are like fingerprints of the states we are looking at. They can tell us, how the interpolators have to be combined to obtain a particular state. Every state is then a well defined mixture of the interpolators used for the correlation matrix.

As an example, we study a  $4 \times 4$  matrix problem. We obtain out of the eigenvalue problem 4 eigenvalues, which we sort according to their size. The biggest eigenvalue corresponds to the ground state, the second largest to the first excitation, etc. The corresponding eigenvectors each have 4 components. As we

know, the correlation matrix has the form

$$C(t)_{ij} = \langle O_i(t) O_j(0)^\dagger \rangle . \quad (8.7)$$

The generalised eigenvalue problem is given by

$$C(t) \vec{v}^{(a)} = \lambda^{(a)} C(t_0) \vec{v}^{(a)} , \quad (8.8)$$

where the superscript  $a$  denotes the  $a^{\text{th}}$  state, which for our example has values  $a = 1, 2, 3, 4$ , and more generally  $a = 1, \dots, n$ . The eigenvectors fulfill the orthogonality relation

$$\vec{v}^{(a)\dagger} C(t_0) \vec{v}^{(b)} = \delta_{ab} . \quad (8.9)$$

We introduce new interpolators  $\tilde{O}$  defined as

$$\tilde{O}^{(a)} = \sum_{i=1}^4 v_i^{(a)*} O_i , \quad a = 1, 2, 3, 4 . \quad (8.10)$$

The correlation matrix of the new interpolator is then given by

$$\begin{aligned} \langle \tilde{O}_i^{(a)}(t) \tilde{O}_j^{(b)}(0)^\dagger \rangle &= \sum_{ij} v_i^{(a)*} v_j^{(b)} \langle O_i(t) O_j(0)^\dagger \rangle \\ &= \vec{v}^{(a)\dagger} C(t) \vec{v}^{(b)} = \vec{v}^{(a)\dagger} \lambda^{(b)} C(t_0) \vec{v}^{(b)} \\ &= \lambda^{(b)} \vec{v}^{(a)\dagger} C(t_0) \vec{v}^{(b)} = \lambda^{(b)} \delta_{ab} . \end{aligned} \quad (8.11)$$

The  $\tilde{O}^{(a)}$  generate orthogonal states and are hence identified as the optimal approximation of the physical states.

Thus, if we plot the entries of the eigenvector  $\vec{v}^{(a)}$ , we can see, how the state number  $a$  is composed from the interpolators  $O_i$ . This means we can find out of which interpolator the state has been mainly built.

In Fig. 8.11 we show the ground state and the excited states eigenvectors as a function of  $t$ , for a  $16 \times 48$  lattice. It is remarkable, that the entries of the eigenvalues are almost independent of  $t$  and form perfect plateaus. These plateaus display how the states are composed from the basis of interpolators. The ground state in Fig. 8.11(a) is dominated by operators  $O_3$  and  $O_5$ , whereas, e.g., the highest excited state in Fig. 8.11(e) is a mixture of all interpolators.

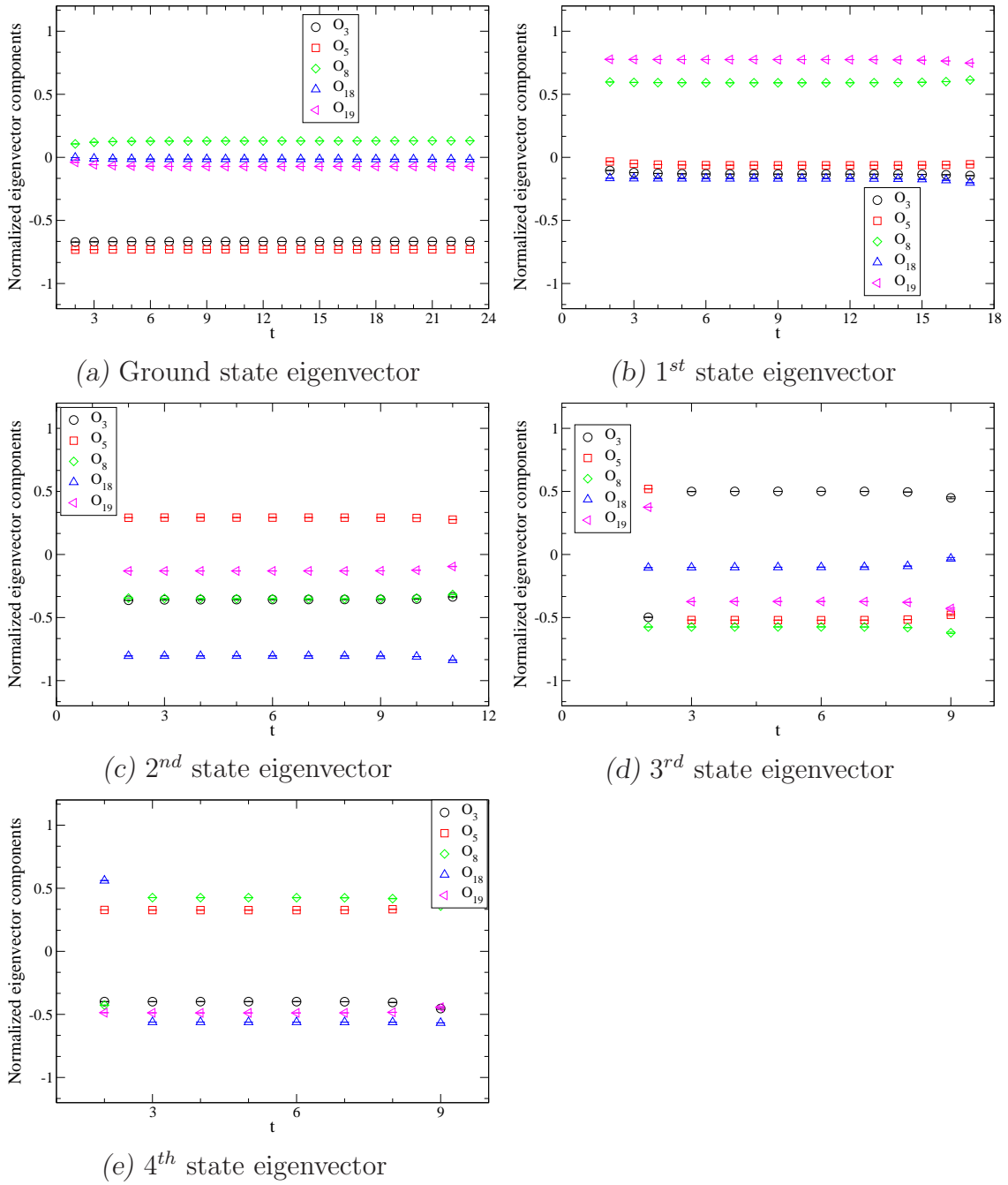
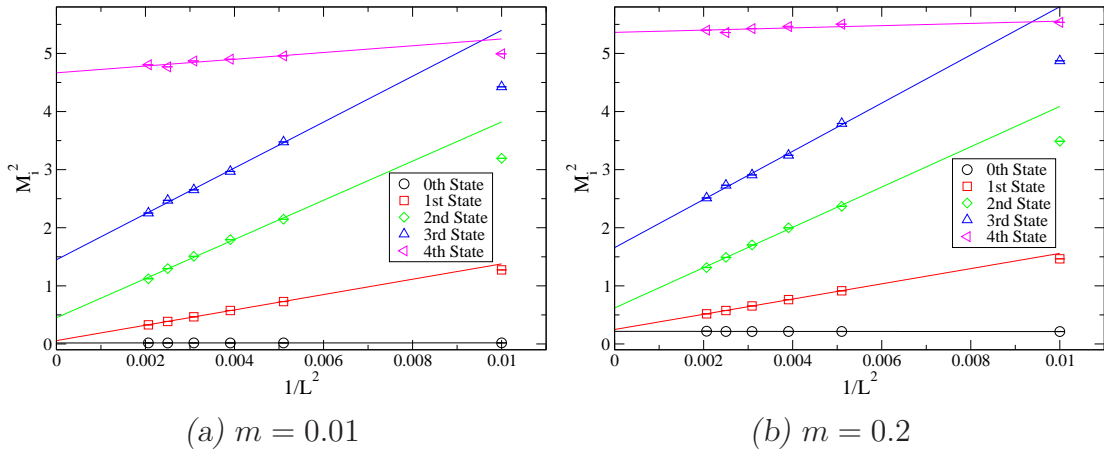


Figure 8.11: Eigenvectors of a  $16 \times 48$  lattice, for  $g = 0.01$  and  $m = 0.05$ .



**Figure 8.12:** Fit of the plots which show the volume dependence of the excited states, each for  $g = 0.05$ .

## 8.7 Extrapolation of the mass spectrum

We are also interested in the extrapolation of the mass spectrum towards infinite volume. Since we plot the inverse of the lattice extension squared, this means extrapolation towards  $1/L^2 \rightarrow 0$ .

In Fig. 8.12 the extrapolation of the states towards  $L \rightarrow \infty$  is shown for two different masses. We use a two-parameter fit,  $y = a_0 + a_1/L^2$ , since there is obviously a linear volume behaviour. The data are perfectly well described by the linear fits which typically have  $\chi^2 \sim 10^{-3}$ .

An overview of the results of the two-parameter fit is given in Tab. 8.1 for  $N_f = 2$  flavors, and in Tab. 8.2 for  $N_f = 6$  flavors. We also indicate whether the state is a bound- or a scattering state. Only for the last state, the 5<sup>th</sup> one, this identification is unclear.

For bound states the fit coefficient  $a_0$  has to be interpreted as the square of the mass

$$a_0 = (m^{(0)})^2, \quad (8.12)$$

while for scattering states it follows from Eq. (8.3) that

$$a_0 = 4 (m^{(i)})^2, \quad i = 1, 2, 3, \quad (8.13)$$

where  $m^{(i)}$  is the mass of the scattering particles (assuming they are of equal mass).

$m$	$n^{\text{th}}$ state	$a_0$	$a_1$	quality
0.01	1	0.01745	0.12229	bound
	2	0.05802	132.012	scattering
	3	0.45086	336.958	scattering
	4	1.44898	394.853	scattering
	5	4.66675	58.191	unclear
0.05	1	0.04416	0.09183	bound
	2	0.08283	132.174	scattering
	3	0.46994	340.524	scattering
	4	1.47780	401.113	scattering
	5	4.78862	58.1538	unclear
0.1	1	0.08990	-0.02594	bound
	2	0.12660	131.956	scattering
	3	0.50763	343.545	scattering
	4	1.52615	407.096	scattering
	5	4.95379	52.8663	unclear
0.2	1	0.21718	-0.37262	bound
	2	0.24879	130.996	scattering
	3	0.62011	346.73	scattering
	4	1.65776	414.556	scattering
	5	5.36260	19.2968	unclear

**Table 8.1:** Table of the fit parameters  $a_0$  and  $a_1$  for the fit of the  $M_i^2$  for  $N_f = 2$ . Also a classification in bound and scattering states is given. The coupling constant is  $g = 0.05$ , and  $m$  denotes the bare mass parameter.

We now study in a joint analysis both the mass  $m^{(0)}$  from the ground state as well as the masses  $m^{(i)}$  which appear in the scattering states. The results are listed in Tab. 8.3 for  $N_f = 2$  flavors, and Tab. 8.4 for  $N_f = 6$  flavors, and are interpreted in Sec. 8.8.

$m$	$n^{\text{th}}$ state	$a_0$	$a_1$	quality
0.01	1	0.17755	0.11031	bound
	2	0.21177	131.328	scattering
	3	0.57990	347.559	scattering
	4	1.44900	450.770	scattering
	5	5.25008	36.6036	unclear
0.05	1	0.23405	-0.11567	bound
	2	0.26628	130.750	scattering
	3	0.63078	348.204	scattering
	4	1.50661	452.696	scattering
	5	5.37933	32.4717	unclear
0.1	1	0.31618	-1.67491	bound
	2	0.33536	132.254	scattering
	3	0.70258	348.277	scattering
	4	1.57804	455.918	scattering
	5	5.58388	13.3954	unclear
0.2	1	0.48997	-1.05615	bound
	2	0.51225	128.100	scattering
	3	0.86843	346.822	scattering
	4	1.74386	459.207	scattering
	5	5.84917	19.4926	unclear

**Table 8.2:** Same as Tab. 8.1, now for  $N_f = 6$ .

## 8.8 Interpretation of the results

We produced data for the 3 different numbers of flavors  $N_f = 2, 4, 6$ . The evaluation of it shows, as can be seen in Fig. 8.13, that the effect of increasing the number of flavors seems to be small. Obviously, the biggest effect is seen for the ground state. The ground state mass increases with the number of flavors. The higher excited states, stay more or less the same, with only a tiny increase of their mass values. We plot the dependence also for different lattice sizes. An exact analysis of the size effects is given in Sec. 8.5. Here, just an overview of the different volumes for the 3 flavors is given. Moreover, Fig. 8.13 compares the

$m$	$n^{\text{th}}$ state	$a_0$	$m^{(i)}$
0.01	1	0.01745	0.13208
	2	0.05802	0.12044
	3	0.45086	0.33572
	4	1.44898	0.60187
0.05	1	0.04416	0.21014
	2	0.08283	0.14390
	3	0.46994	0.34276
	4	1.47780	0.60786
0.1	1	0.08990	0.299835
	2	0.12660	0.177902
	3	0.50763	0.356240
	4	1.52615	0.617688
0.2	1	0.21718	0.466026
	2	0.24879	0.249392
	3	0.62011	0.393737
	4	1.65776	0.643770

**Table 8.3:** Table of the mass value  $m^{(i)}$  calculated out of the fit parameter  $a_0$ . The coupling constant is  $g = 0.05$ , and  $m$  is the bare mass parameter. These results are for  $N_f = 2$ .

two masses  $m = 0.01$  and  $m = 0.2$  with each other. We see once again, that the ground state changes the most. The excited states, do not vary much.

In the previous Section 8.7 we have also extracted the masses  $m^{(i)}$  of individual particle excitations. The results of the mass values  $m^{(i)}$ , presented in Tab. 8.3 and Tab. 8.4, are now plotted as a function of the bare mass  $m$  in Fig. 8.14(a) ( $N_f = 2$ ) and Fig. 8.14(b) ( $N_f = 6$ ). We see that all  $m^{(i)}$  show a linear dependence on the parameter  $m$ . It is interesting to observe that the state  $m^{(0)}$  which comes from the smallest value  $M_0$  (black line) is shifted upwards considerably for the large value of  $N_f$ . Furthermore,  $m^{(0)}$  shows a slope which is roughly twice as big as the slope for the other masses.

The mass  $m^{(0)}$  is mainly influenced by the three following aspects:

1. It comes from a state which shows no  $L$ -dependence,

$m$	$n^{\text{th}}$ state	$a_0$	$m^{(i)}$
0.01	1	0.17755	0.42136
	2	0.21177	0.23009
	3	0.57990	0.38076
	4	1.44900	0.60187
0.05	1	0.23405	0.48379
	2	0.26628	0.25801
	3	0.63078	0.39711
	4	1.50661	0.61372
0.1	1	0.31618	0.56230
	2	0.33536	0.28955
	3	0.70258	0.41910
	4	1.57804	0.62810
0.2	1	0.48997	0.69998
	2	0.51225	0.35786
	3	0.86843	0.46595
	4	1.74386	0.66028

**Table 8.4:** Same as Tab. 8.3, now for  $N_f = 6$ .

2. it has a steeper slope as a function of  $m$  and
3. it shows a strong shift in  $N_f$ .

Thus, we conclude that  $m^{(0)}$  is of different type than the  $m^{(i)}$ ,  $i \neq 0$ . For the clarification of the nature of this state further studies are in preparation.

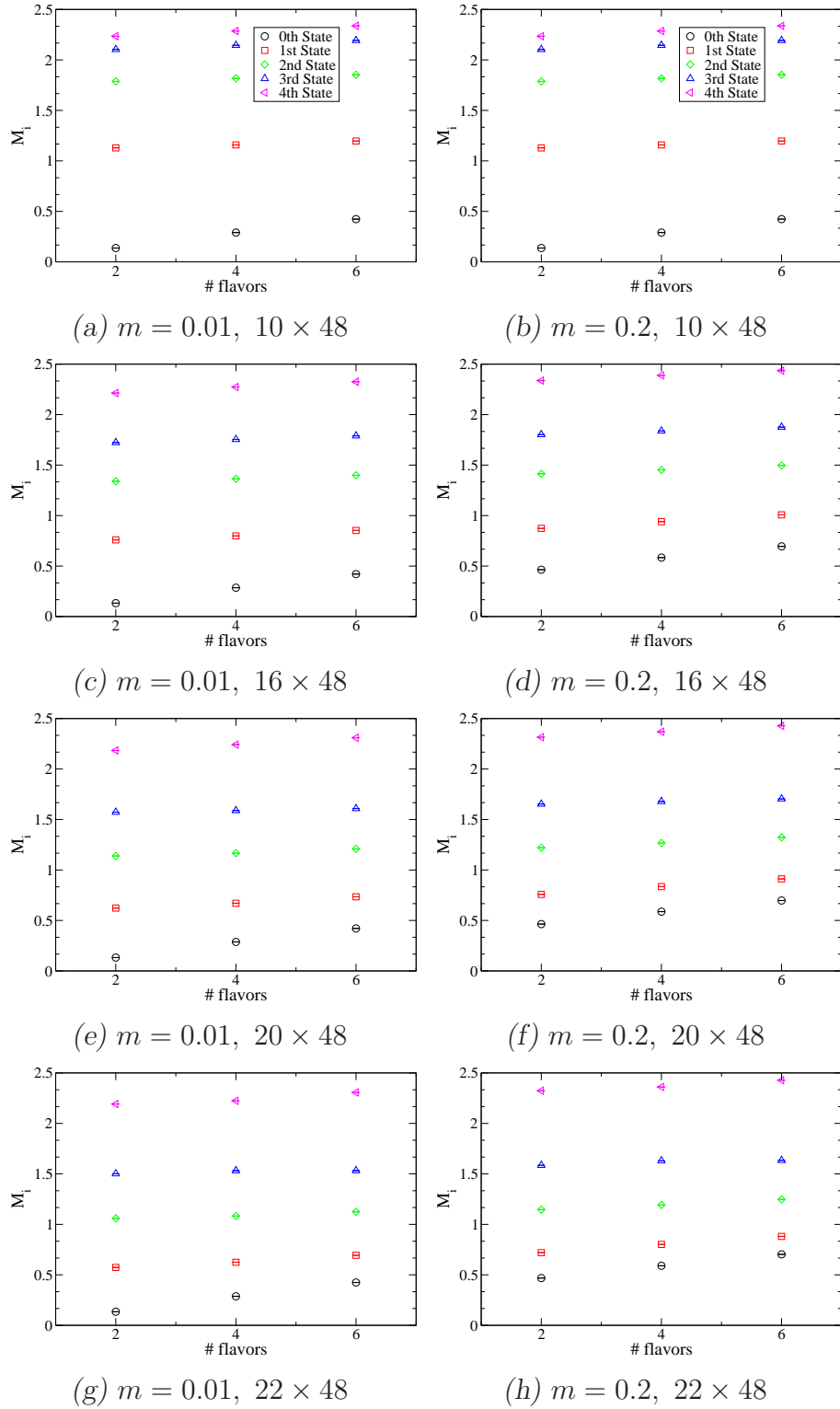


**Figure 8.13:** Plot of the flavor dependence of  $M_i$  compared for two different masses and different lattice sizes, each for  $g = 0.05$ , the legend for each column is only given in the uppermost figure.

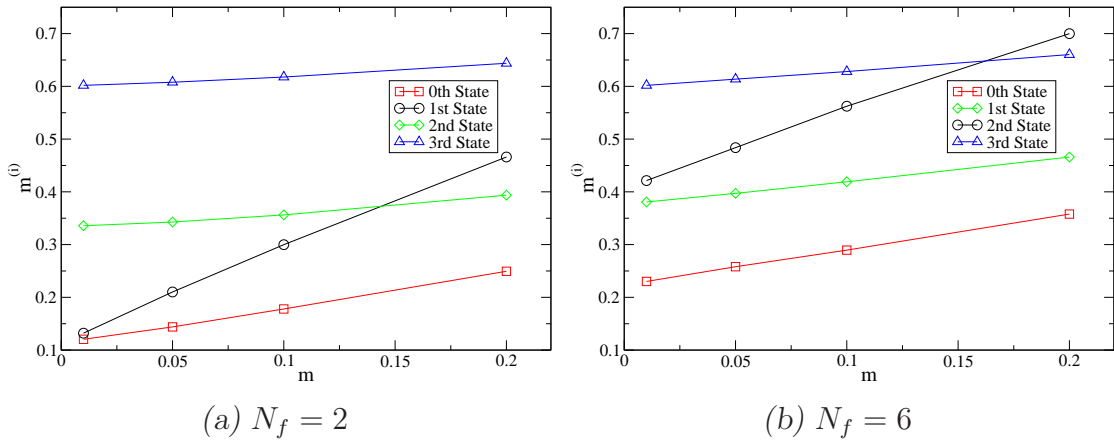


**Figure 8.14:** The plots show the dependence of the mass value  $m^{(i)}$  on the bare mass  $m$  for the coupling constant  $g = 0.05$ , compared for two different flavors (the points are connected to guide the eye).

## 8.9 Table for the mass values

To give a brief overview, we present a table with values of  $M_i$  for different lattice sizes:

$L$	$n^{\text{th}}$ state	$M_i$
$10 \times 48$	1	0.2996(09)
$10 \times 48$	2	1.1608(03)
$10 \times 48$	3	1.8235(04)
$10 \times 48$	4	2.1529(04)
$10 \times 48$	5	2.2920(06)
$14 \times 48$	1	0.3000(07)
$14 \times 48$	2	0.8933(03)
$14 \times 48$	3	1.4961(05)
$14 \times 48$	4	1.9026(05)
$14 \times 48$	5	2.2847(07)
$16 \times 48$	1	0.2986(09)
$16 \times 48$	2	0.8028(03)
$16 \times 48$	3	1.3696(02)
$16 \times 48$	4	1.7582(04)
$16 \times 48$	5	2.2729(22)
$18 \times 48$	1	0.2993(07)
$18 \times 48$	2	0.7320(03)
$18 \times 48$	3	1.2588(03)
$18 \times 48$	4	1.6621(05)
$18 \times 48$	5	2.2659(06)
$20 \times 48$	1	0.2992(06)
$20 \times 48$	2	0.6753(03)
$20 \times 48$	3	1.1707(03)
$20 \times 48$	4	1.6064(03)
$20 \times 48$	5	2.2465(05)
$22 \times 48$	1	0.3011(06)
$22 \times 48$	2	0.6304(03)
$22 \times 48$	3	1.0920(03)
$22 \times 48$	4	1.5359(03)
$22 \times 48$	5	2.2546(02)

**Table 8.5:** Selected mass values for different lattice extensions  $L$ , with the coupling constant  $g = 0.05$ , the bare mass  $m = 0.1$ , and for  $N_f = 2$ .

# Chapter 9

## Summary and outlook

Often, when starting with a new innovative project, one does not foresee, how far it will lead. To a certain extent this was the case with this work. The original goal was to study the Gross-Neveu model in the large  $N_f$  limit, but instead many interesting insights on techniques for excited state spectroscopy were obtained. Here we summarise these results, present our conclusions and discuss possible topics for further studies.

### Summary

The main focus of this work was the analysis of the excited states in the Gross-Neveu model on the lattice, and the improvement of the corresponding techniques. Furthermore we were interested in a dynamical simulation of the fermions for various numbers of flavors.

The dynamics of the fermions was implemented with the Hybrid Monte-Carlo method. It fully includes the fermion determinant in the simulations. For rewriting the determinant we had to introduce pseudofermion fields, which are essentially bosons. The update of the scalar field which generates the 4-fermi interaction, was done with the molecular dynamics leapfrog evolution. The various numbers of flavors were obtained by introducing  $N_f/2$  pseudoscalar fields for the case of  $N_f$  flavors ( $N_f$  even). As a test for the correctness of the HMC update, the configurations of the scalar field were compared to the output of an independently written program.

When having produced configurations of the scalar field, we started with the second part of this diploma thesis, the study of excited states. As technique to obtain the excitations of the mass spectrum we used the variational method. It extracts the states out of a correlation matrix. This matrix correlates interpolators which describe the desired state, i.e., have the correct quantum numbers. For optimal results we put much effort in the construction of good basis interpolators. The main idea here was, to introduce new types of interpolators with displaced sources. We used interpolators with relative plus signs, but also ones with relative minus signs. Especially the ones with a relative minus sign, which correspond to interpolators with derivatives, brought us an immense step forward in our analysis, since they are the ones which couple to higher excitations.

The correlation matrix was built out of a total of 18 interpolators. The implementation of this matrix has been tested with another computer program which analysed the free case, where the coupling constant  $g$  is equal to zero and where Fourier transformation can be applied. Furthermore, the hermiticity of the correlation matrix within error bars was checked, which is another test of the correctness of the matrix.

The last part of this work dealt with the analysis of the data. An important aspect is that when obtaining the excited states out of the correlation matrix, we only use a subset of the available interpolators. The choice which interpolators should be put into the correlation matrix, was a difficult question. We observed, that much can be gained by looking at the diagonal entries of the correlation matrix. There we could see which interpolators show a steeper slope, and hence, couple to higher excitations. We noticed, that the newly introduced types of interpolators with a displaced source, couple strongly to the higher excited states. When looking at a lattice with a time extension of  $L_t = 64$ , we checked, that they all also couple to the ground state as it should be. Also the eigenvectors of the generalised eigenvalue problem, which are like a fingerprint for the states, confirmed that always the displaced source interpolators are predominantly involved in building up the higher excited states.

From the eigenvalues of the correlation matrix, through the variational method, we obtained effective mass plateaus. The quality of the plateaus provides a criterion for a good choice of interpolators. Finding long plateaus with small error bars, told us that a combination of interpolators represents a physical

state properly. We managed to get up to five states.

We were also interested in the dependence of the mass spectrum on the bare mass  $m$ . By studying it, we found out, that the effect of varying the parameter  $m$  was very small. For a fixed coupling  $g$ , the spectrum is essentially a linear function of  $m$ .

When we started with this project we did not foresee that we would find scattering states as well. For the examination of the finite size effects, characteristic for scattering states, we simulated lattice sizes of  $10 \times 48$ ,  $14 \times 48$ ,  $16 \times 48$ ,  $18 \times 48$ ,  $20 \times 48$  and  $22 \times 48$ . We observed that some of the excited states were volume dependent. Since scattering states show such a volume dependence, this led to the conclusion that some of the excitations correspond to scattering states. Only for our highest excited state it is still unclear whether it is a bound state or a scattering state.

The identification of the scattering states on different volumes was done via the eigenvectors. Using them we could match the different states for various lattice sizes. This shows us, that the eigenvectors are a very important tool in the analysis.

As mentioned before, the HMC also made it possible to simulate various numbers of flavors. In our case we simulated  $N_f = 2, 4, 6$ . We can conclude that the influence of flavor seems to be small. Only the ground state shows an increasing mass as  $N_f$  is increased.

Finally, we also calculated the mass value  $m^{(0)}$  for the bound state as well as the masses  $m^{(1)}, \dots, m^{(3)}$  of the scattering partners in the scattering states out of a fit for large  $L$ . Plotting the mass results as a function of the bare mass  $m$ , we observed especially in the comparison for two different numbers of flavors, some interesting new findings. First of all, all the states depend on  $m$  linearly. Secondly, the bound state clearly is of different nature compared to the other states. It shows a much steeper slope than the others and is more affected by increasing the numbers of flavors. Finally, it is the only state that did not show volume dependence. For a detailed clarification of the nature of this state further studies have to be done.

To summarise, the main effort has been put into three parts. In the first one, we simulated dynamical fermions for  $N_f$  flavors with the HMC algorithm. In the second part, we were busy with the construction of good basis interpolators and

the development of the code to correlate them. The last part was, of course, the analysis and the understanding of the results.

## **Outlook**

As in every work where only limited time is available, the studies can be improved. Especially larger lattices where more extended interpolators are possible will help in the understanding of the scattering states. The identification of them has not been completely clear for the higher states. In particular, for the highest observed state (5<sup>th</sup> one), it is open whether it is a stable excited state or a scattering state.

Furthermore, a bigger variety of interpolators would help particularly in the above mentioned problem. More interpolators could possibly mean the identification of more excited states. If we would find a sixth excitation, it would certainly settle some questions.

Unknown is also if there exist further bound states. Again, larger lattice sizes and more interpolators would help in the understanding.

Of course raising the numbers of flavors would be of high interest. With a maximum of  $N_f = 6$  flavors, it is not quite possible to verify the statement about the large  $N_f$  limit of Sec. 2.3. For large  $N_f$ , however, the behaviour of the energy spectrum is known exactly and it would be interesting to see how large  $N_f$  has to become in practice.

Moreover, increasing the numbers of flavors would help in the clarification of the bound state we found. Since the state is strongly influenced by the numbers of flavors, it would be interesting to observe what happens when data for larger values of  $N_f$  are analysed.

# Appendix A

## Fourier transformation on the lattice

We here want to present the basic formulas for Fourier transformation on the lattice. The lattice is defined as

$$\Lambda = \{\mathbf{n} = (n_1, n_2) \mid n_\mu = 0, \dots, L_\mu - 1\} , \quad (\text{A.1})$$

with  $\mathbf{n}$  being the vector which points to each lattice site. The volume of the lattice is  $V = L_1 L_2$ . If we consider now a function  $f(\mathbf{n})$  on this lattice it obeys toroidal boundary conditions in both directions  $\mu$ ,

$$f(\mathbf{n} + \hat{\mu} L_\mu) = e^{2\pi i \vartheta_\mu} f(\mathbf{n}) . \quad (\text{A.2})$$

$\hat{\mu}$  denotes the unit-vector in  $\mu$ -direction and  $\vartheta_\mu = 0$  for periodic boundary conditions, or  $\vartheta_\mu = 1/2$  for anti-periodic boundary conditions. The lattice in momentum space is given by

$$\tilde{\Lambda} = \{\mathbf{p} = (p_1, p_2) \mid p_\mu = \frac{2\pi}{aL_\mu} (k_\mu + \vartheta_\mu), k_\mu = 0, \dots, L_\mu - 1\} . \quad (\text{A.3})$$

The most important formula for a Fourier transformation on the lattice is

$$\frac{1}{N} \sum_{k=0}^{N-1} \exp\left(i \frac{2\pi}{N} l \cdot k\right) = \delta_{l,k} , \quad (\text{A.4})$$

with  $l$  being an integer between  $0 \leq l \leq N - 1$ . From that we can derive the following useful expressions:

$$\frac{1}{V} \sum_{\mathbf{p} \in \tilde{\Lambda}} \exp(i\mathbf{p}[\mathbf{n} - \mathbf{m}]a) = \delta(\mathbf{n} - \mathbf{m}) = \delta_{n_1, m_1} \delta_{n_2, m_2} , \quad (\text{A.5})$$

$$\frac{1}{V} \sum_{\mathbf{n} \in \Lambda} \exp(i[\mathbf{p} - \mathbf{q}]\mathbf{n}a) = \delta(\mathbf{p} - \mathbf{q}) . \quad (\text{A.6})$$

We now apply Fourier transformation on the function  $f(\mathbf{n})$  and obtain

$$\tilde{f}(\mathbf{p}) = a^2 \frac{1}{\sqrt{V}} \sum_{\mathbf{n} \in \Lambda} f(\mathbf{n}) \exp(-i\mathbf{p}\mathbf{n}a) . \quad (\text{A.7})$$

The inverse transformation then is

$$f(\mathbf{n}) = \frac{1}{a^2 \sqrt{V}} \sum_{\mathbf{p} \in \tilde{\Lambda}} \tilde{f}(\mathbf{p}) \exp(i\mathbf{p}\mathbf{n}a) . \quad (\text{A.8})$$

The last equation can easily be received by inserting (A.7) in (A.8) and using (A.5).

# Appendix B

## The 2-dimensional representation of the $\gamma$ -matrices

The Minkowski  $\gamma$ -matrices in 4 dimensions obey the relation

$$\{\gamma_\mu^M, \gamma_\nu^M\} = 2 g_{\mu\nu} \mathbb{1} , \quad (\text{B.1})$$

with  $\mu = 0, 1, 2, 3$  and the metric tensor  $g_{\mu\nu} = \text{diag}(1, -1, -1, -1)$ . We can construct the Euclidean gamma matrices ( $\mu = 1, 2, 3, 4$ ) out of the Minkowski matrices by setting  $\gamma_i = -i\gamma_i^M, i = 1, 2, 3$  and  $\gamma_4 = \gamma_0$ . The Euclidean matrices follow the anti-commutating relations

$$\{\gamma_\mu, \gamma_\nu\} = 2 \delta_{\mu\nu} \mathbb{1} . \quad (\text{B.2})$$

The matrix  $\gamma_5$  is defined as the product  $\gamma_5 = \gamma_1\gamma_2\gamma_3\gamma_4$  and obeys  $\gamma_5^2 = \mathbb{1}$  and anticommutes with all the other gamma matrices.

In two dimensions a representation of the Euclidean gamma matrices are the Pauli matrices. We obtain

$$\gamma_1 = \sigma_1 = \begin{pmatrix} 0 & 1 \\ 1 & 0 \end{pmatrix} , \quad \gamma_2 = \sigma_2 = \begin{pmatrix} 0 & -i \\ i & 0 \end{pmatrix} , \quad \gamma_5 = \sigma_3 = \begin{pmatrix} 1 & 0 \\ 0 & -1 \end{pmatrix} . \quad (\text{B.3})$$

As we can easily see, they obey the Clifford algebra

$$\{\gamma_\mu, \gamma_\nu\} = 2 \delta_{\mu\nu} \mathbb{1} , \quad (\text{B.4})$$

and

$$\gamma_\mu = \gamma_\mu^\dagger , \quad \{\gamma_\mu, \gamma_5\} = 0 , \quad \gamma_5^2 = \mathbb{1} . \quad (\text{B.5})$$

In the discussion of the charge conjugation we need to know the charge conjugation matrix  $C$ . The defining relation for this matrix is

$$C \gamma_\mu C^{-1} = -\gamma_\mu^T . \tag{B.6}$$

In 2 dimensions a possible choice is  $C = i\gamma_2$ , so that  $C = -C^{-1}$ . If we insert  $\gamma_{1,2}$  in (B.6) we see that this relation holds.

# Appendix C

## Discussion of the correlation matrix

A list of the functional form of the correlation matrix is given in Tab. C.1. An important check if the entries of the correlation matrix are correct, is to prove hermiticity. The relation

$$C_{ij} = C_{ji}^* \quad (\text{C.1})$$

has to be fulfilled. In addition to that, the diagonal elements of the correlation matrix have to have a cosh-form, which also is satisfied.

$i   j$	(1)	(2)	(3)	(4)	(5)	(6)	(8)	(9)	(10)
(1)	c	is	c	is	c	is	-is	c	-is
(2)	-is	c	-is	c	-is	c	c	-is	-c
(3)	c	is	c	is	c	is	-is	c	-is
(4)	-is	c	-is	c	-is	c	c	-is	-c
(5)	c	is	c	is	c	is	-is	-c	is
(6)	-is	c	-is	c	-is	c	-c	-is	c
(8)	is	c	is	c	is	-c	c	-is	-c
(9)	c	is	c	is	-c	-is	is	c	-is
(10)	is	-c	is	-c	-is	c	-c	is	c

**Table C.1:** Functional form of the the correlation matrix  $\langle C_{ij}(t) \rangle$ .  $i$  and  $j$  denote the index and hence the operator, which has been implemented in the matrix. The symbol "c" stands for cosh and the symbol "is" stands for the imaginary unit times sinh.



# References

- [1] J. Danzer and C. Gattringer, *Excited state spectroscopy in the lattice Gross-Neveu model*, *PoS LAT2007*, 092 (2007).
- [2] C. Michael, *Adjoint sources in lattice gauge theory*, *Nucl. Phys.* **B259**, 58–76 (1985).
- [3] M. Lüscher and U. Wolff, *How to calculate the elastic scattering matrix in two-dimensional quantum field theories by numerical simulation*, *Nucl. Phys.* **B339**, 222–252 (1990).
- [4] R. F. Dashen, B. Hasslacher, and A. Neveu, *Semiclassical bound states in an asymptotically free theory*, *Phys. Rev.* **D12**, 2443–2458 (1975).
- [5] A. B. Zamolodchikov and A. B. Zamolodchikov, *Exact S matrix of the Gross-Neveu “elementary” fermions*, *Phys. Lett.* **B72**, 481–483 (1978).
- [6] J. E. Hirsch, *Discrete Hubbard-Stratonovich transformation for fermion lattice models*, *Phys. Rev.* **B28**, 4059–4061 (1983).
- [7] J. E. Hirsch, *Erratum: Discrete Hubbard-Stratonovich transformation for fermion lattice models*, *Phys. Rev.* **B29**, 4159 (1984).
- [8] D. J. Gross and A. Neveu, *Dynamical symmetry breaking in asymptotically free field theories*, *Phys. Rev.* **D10**, 3235–3253 (1974).
- [9] R. Kenna and J. C. Sexton, *The weakly coupled Gross-Neveu model with Wilson fermions*, *Phys. Rev.* **D65**, 014507 (2002).
- [10] W. E. Thirring, *A soluble relativistic field theory*, *Annals Phys.* **3**, 91–112 (1958).

- [11] Y. Nambu and G. Jona-Lasinio, *Dynamical model of elementary particles based on an analogy with superconductivity. I*, *Phys. Rev.* **122**, 345–358 (1961).
- [12] Y. Nambu and G. Jona-Lasinio, *Dynamical model of elementary particles based on an analogy with superconductivity. II*, *Phys. Rev.* **124**, 246–254 (1961).
- [13] N. D. Mermin and H. Wagner, *Absence of ferromagnetism or antiferromagnetism in one- dimensional or two-dimensional isotropic Heisenberg models*, *Phys. Rev. Lett.* **17**, 1133–1136 (1966).
- [14] S. R. Coleman, *There are no Goldstone bosons in two-dimensions*, *Commun. Math. Phys.* **31**, 259–264 (1973).
- [15] P. C. Hohenberg, *Existence of Long-Range Order in One and Two Dimensions*, *Phys. Rev.* **158**, 383–386 (Jun, 1967).
- [16] M. Limmer, *Lattice simulation of the Gross-Neveu model*. Master thesis, 2006.
- [17] C. Gattringer, V. Hermann, and M. Limmer, *Fermion loop simulation of the lattice Gross-Neveu model*, *Phys. Rev.* **D76**, 014503 (2007).
- [18] P. de Forcrand and U. Wenger, *New baryon matter in the lattice Gross-Neveu model*, *PoS LAT2006*, 152 (2006).
- [19] F. Knechtli, T. Korzec, B. Leder, and U. Wolff, *Universality in the Gross-Neveu model*, *Nucl. Phys. Proc. Suppl.* **140**, 785–787 (2005).
- [20] T. Korzec, F. Knechtli, U. Wolff, and B. Leder, *Monte-Carlo simulation of the chiral Gross-Neveu model*, *PoS LAT2005*, 267 (2006).
- [21] T. Korzec and U. Wolff, *Gross-Neveu model as a laboratory for fermion discretization*, *PoS LAT2006*, 218 (2006).
- [22] C. Gattringer and C. B. Lang, *QCD on the lattice – an introduction for beginners*. Unpublished notes.

- 
- [23] I. Montvay and G. Münster, *Quantum fields on a lattice*. Cambridge, UK: Univ. Pr. (1994) 491 p. (Cambridge Monographs on Mathematical Physics).
- [24] J. Smit, *Introduction to quantum fields on a lattice: A robust mate*, *Cambridge Lect. Notes Phys.* **15**, 1–271 (2002).
- [25] J. Zinn-Justin, *Quantum Field Theory and Critical Phenomena*. Oxford University Press, New York, 2002.
- [26] K. G. Wilson, *Confinement of quarks*, *Phys. Rev.* **D10**, 2445–2459 (1974).
- [27] S. Aoki and K. Higashijima, *The recovery of the chiral symmetry in lattice Gross-Neveu model*, *Prog. Theor. Phys.* **76**, 521 (1986).
- [28] <http://www.netlib.org/lapack/>
- [29] G. C. Wick, *The Evaluation of the Collision Matrix*, *Phys. Rev.* **80**, 268–272 (1950).
- [30] T. Burch, C. Gatttringer, L. Y. Glozman, C. Hagen, and C. B. Lang, *Variational method for lattice spectroscopy with ghosts*, *Phys. Rev.* **D73**, 017502 (2006).
- [31] M. Lüscher, *Volume Dependence of the Energy Spectrum in Massive Quantum Field Theories. 2. Scattering States*, *Commun. Math. Phys.* **105**, 153–188 (1986).
- [32] M. Lüscher, *On a relation between finite size effects and elastic scattering processes*, . Lecture given at Cargese Summer Inst., Cargese, France, Sep 1-15, 1983.
- [33] M. Lüscher, *Signatures of unstable particles in finite volume*, *Nucl. Phys.* **B364**, 237–254 (1991).



# Danksagung

Meinen besonderen Dank möchte ich meinem Betreuer Christof Gattringer aussprechen. Er hat mir etwas Bedeutendes vermittelt: die Freude an der Arbeit. Selbst wenn er Stress hat, nimmt er sich die Zeit um etwas geduldig zu erklären. Es hat immer Spaß gemacht, zu ihm zu gehen. Vor allem, er weiß auch, dass es auch noch andere Dinge als Physik im Leben gibt. Ich kann mir wirklich keinen besseren Betreuer für meinen Einstieg in die Physik vorstellen.

Zu meiner Arbeit haben auch mehrere Leute beigetragen. Ein ganz großer Dank gebührt dabei Daniel Mohler. Dessen ausgereiftes Analyseprogramm hat mir, und auch anderen Kollegen, viel Arbeit abgenommen und auch Zeit erspart.

Weiters danke ich Martin Schwinzerl, der mir mit seinem enormen Computerverwissen immer wieder bei kleineren Problemen geholfen hat.

Und zuletzt, aber doch am entscheidendsten, danke ich Markus Limmer. Auf dessen Arbeit, "Lattice simulation of the Gross-Neveu model", baut meine auf. Er hat mich eingewiesen, meine Arbeiten korrigiert und war immer da, falls ich Fragen hatte.

Eine Diplomarbeit hat Höhen und Tiefen. Trotz allem, gibt es Menschen die mich immer unterstützt haben. Darunter zählen drei im Besonderen: Mein Vater und meine Mutter, Robert und Brigitte Danzer, und mein Partner, Markus Limmer. Ihnen möchte ich danken für ihre Geduld, ihren Zuspruch und das Vertrauen dass sie in mich gesteckt haben.

Zwei Leute möchte ich noch erwähnen. Es sind für mich ganz besondere Freunde, die mir immer geholfen und zugehört haben. Auch moralische Unterstützung ist eine Art von Hilfe. Ich danke Andreas und Markus H. für ihre Freundschaft.